This is a repository copy of *An analytical model for lateral depth-averaged velocity distributions along a meander in curved compound channels*.

Article:

An analytical model for lateral depth-averaged velocity distributions along a meander in curved compound channels

Chao Liu[a, b], Nigel Wright[c], Xingnian Liu[a,b] , Kejun Yang[a,b,*]

[a]State Key Laboratory of Hydraulics and Mountain River Engineering, Sichuan University, Chengdu, Sichuan 610065, China

[b]College of Water Resources and Hydropower, Sichuan University, Chengdu, Sichuan 610065, China

[c]School of Civil Engineering, University of Leeds, Leeds LS2 9JT, UK

[*]Corresponding author. Tel.: +86 28 85401937.
E-mail address: yangkejun@scu.edu.cn (K. Yang).

Abstract: This paper presents an analytical method for modeling the lateral depth-averaged velocity distribution along a half-meander in a curved compound channel. An equation is derived from the momentum equation and the flow continuity equation which contains a velocity term with both streamwise velocity variation and lateral secondary flow variation. A velocity variation parameter is proposed in the main channel and on the floodplain for a series of test sections. To study the validity of these equations experiments were conducted in a large scale meandering compound channel at Sichuan University, China. Based on the experimental data, the generation mechanism of secondary flow in the main channel along half a meander is analyzed. It is shown that the secondary current is enhanced by the centrifugal force and the floodplain flow. Due to the discontinuity of the flow depth and the effect of meandering in the main channel flow, a region divided method is adopted. A new boundary condition is proposed by introducing the angle between the main channel flow and the floodplain flow, and it is shown that this gives better modeling results in cross-over sections. The modeling results indicate that the proposed method,

which uses the new boundary condition and includes both the streamwise velocity variation and the lateral secondary flow variation, can model the lateral depth-averaged velocity distributions more accurately. Finally, variations in the velocity term between the main channel and floodplain are discussed and analyzed.

Key words: meandering compound channel, secondary flow generation mechanism, divided region method, two-dimensional model, boundary condition

1. Introduction

In a river corridor system, rivers play an important role in the provision of water and habitat to the surrounding fauna and flora. Natural alluvial rivers and streams often exhibit a curved main river and one or two corresponding floodplains. When a flood occurs, the flow depth increases and the floodplains are submerged to convey the extra flow, leading to overbank flow in the meandering compound channel. It is important to note that the flow characteristics in a curved channel are very different to that in a straight one, especially with regard to the generation mechanism of main channel secondary flows. Accordingly, it is necessary to assess the changes of the velocity, secondary flow, bed shear stress and discharge in the meandering compound channels.

To determine sediment transport, channel morphology and bank erosion, the lateral distributions of depth-averaged velocity and bed shear stress are crucial. In recent decades, the three-dimensional flow structure, turbulence characteristics and secondary flows in straight compound channels have been extensively investigated by, amongst others, Knight and Demetriou [14], Pasche and Rouve [25], Knight and Sellin [15], Tominaga et al. [41], Yuen [45], Carling et al.

[3] and Yang et al. [43]. Moreover, lateral distribution methods (LDM) for the depth-averaged velocity and bed shear stress, along with the secondary flow and the planform vorticity, have been developed by Shiono and Knight [31], Cao et al. [2], Rameshwaran and Shiono [29], Huai et al. [9], Hu et al. [8]，Liu et al. [20] and Yang et al. [44]. These researchers showed that the secondary flows affect the predictions of velocity and bed shear stress significantly and ignoring them leads to poor results. Therefore, Ervine et al. [5], Spooner [38] and Huai et al. [10] proposed new secondary flow expressions which were applied at the apex sections in the meandering compound channel with non-mobile bed and mobile bed. However, when the flow depth is discontinuous at the interfaces of main channel and its corresponding floodplains the boundary condition must be reconsidered. Knight et al. [16] and Tang and Knight [39] discussed the boundary conditions for the Shiono and Knight Method [31] (hereafter referred as SKM) and discovered that improved results were obtained by using the continuity of depth-averaged shear stress at the interfaces of main channel and floodplain. Furthermore, the turbulent transfer is also an important phenomenon in compound channels and based on mathematical integration, Castanedo et al. [4] identified three different forms of the turbulent diffusion term in the depth-averaged Navier-Stokes equation. Subsequently, these three models and the original SKM were compared by Tang and Knight [40] in both a straight trapezoidal channel and a straight compound channel. Their conclusions show that to obtain good predictions the four models must contain the secondary flow parameter and this affects the results more than the dimensionless eddy viscosity for overbank flows.

For overbank flow in a meandering compound channel with a fixed bed, experimental work (Shiono and Muto [32], Shiono et al. [33] and Rameshwaran et al. [28]) has shown that secondary

current cells in the main channel are much stronger than those on the floodplain due to the effect

of centrifugal force. For overbank flows in a meandering compound channel, discharge assessment

methods have been proposed by various authors (Greenhill and Sellin [7], Lambert and Sellin [19],

Shiono et al. [34], Patra and Kar [26] and Patra et al. [27]). Flow characteristics were also

discussed in a meandering compound channel with non-mobile bed and three different sinuosities

(1.093~1.571) by Shiono and Muto [32], who found that the secondary flow for the inbank and

overbank flows originated from different mechanisms. Their experimental results also showed that

a strong intensity of secondary current cells existed mainly in the main channel, especially for the

overbank flow. Then, experimental research was extended to curved channels with mobile bed and

different floodplain vegetation by Ishigaki et al. [11], Lyness et al. [21], Keevil et al. [13], Shiono

et al. [35] and Shiono et al. [36, 37]. From these studies, some conclusions were obtained: (1) the

vegetation on the floodplain reduced the channel conveyance capability significantly; (2) the

lateral secondary flow distributions in a meandering channel were quite different between the

cases with the non-mobile bed and mobile bed; (3) in the cases with a mobile bed, multiple

secondary current cells which cause a series of wavy bedforms occur at deeper flow depth along

the meandering main channel when the floodplain roughness increases. These phenomena are

usually seen in natural rivers and the conclusions are therefore valuable for engineering projects.

As well as experimental studies, numerical investigations can also give insight into flows in

meandering channels. A one-dimensional simulation with vegetation in a curved channel was

presented by Martin-Vide et al. [22] and two-dimensional models were described by Shao et al.

[30] and Zarrati et al. [46], presenting good modeling results for the velocity distribution, the

secondary flow and the flow depth. Morvan et al. [24] and Jing et al. [12] carried out three-dimensional methods to simulate the velocity fields in overbank flow. Further, analytical methods have been proposed by Ervine et al. [6], McGahey et al. [23] and Huai et al. [10], based on the SKM method, to predict the depth-averaged velocity distribution. Although velocity patterns in a meandering compound channel are highly three dimensional, these researchers neglected the streamwise velocity variation to simplify the analytical models which were therefore only applicable at apex sections. Knight et al. [18] pointed out that the modeling capability of SKM is poor in meandering compound channels because of the methodology is derived for steady flows in straight prismatic channels. According to the research described above, it is hard to find a reasonable analytical method to predict the lateral velocity distributions along a meander, and the lack of detailed experimental data also presents difficulties. This forms the motivation for this paper in which a new model is presented along with a series of experiments to demonstrate its derivation and validate its results.

The research presented in this paper explores an analytical method to model the depth-averaged velocity along a meander in a curved compound channel. A governing equation is derived from the streamwise momentum equation and the flow continuity equation. Its velocity term contains the streamwise velocity variation, ignored by Ervine et al. [6], McGahey et al. [23] and Huai et al. [10], and the lateral secondary flow variation. In order to verify this model, two groups of experiments were conducted in a large scale meandering compound channel at Sichuan University in China. The three-dimensional velocities, the flow depth and the Reynolds shear stress were recorded at seven test sections along half a meander. Based on the experimental data, the

generation mechanism of secondary flows, including the effects of centrifugal force and floodplain flow, is analyzed and an expression for the velocity variation parameter at the apex and cross-over sections is proposed. Further, the divided method in half a meander is presented by considering the effect of meandering main channel flow. A new boundary condition is proposed by introducing the angle between the main channel and floodplain. Finally, the modeling results of depth-averaged velocity by this method are compared with the experimental data. Each part of the velocity term is discussed and analyzed in the meandering main channel and on the floodplain.

2. Experimental arrangement and apparatus

Two groups of experiments (MN1 and MN2) were conducted in a 35m long, 4m wide and 1m high flume, at State Key Laboratory of Hydraulics and Mountain River Engineering (SKLH), Sichuan University (see Fig.1). The flow depths of MN1 and MN2 in the main channel are 0.255m and 0.216m, respectively. Measurements were carried out for the stage-discharge curve, the Reynolds shear stresses and the three-dimensional velocities. The discharge was measured by a triangular weir installed in front of the flume and the flow depth was measured by an Automatic Ultrasonic Measurement System (AUMS) produced by the Sinfotek Corporation (www.sinfotek.com). The three-dimensional velocities and Reynolds shear stresses were recorded by the three-component Sontek acoustic Doppler velocimeter (ADV), equipped with up-side and down-side probes. At each point, measurement time and frequency were set as 30s and 50Hz, respectively.

The shape of the main channel was rectangular with the vertical side slope and the sinuosity of the meandering main channel was designed as 1.381. The total width (B) and main channel width (b) were 4m and 0.7m, respectively with the main channel depth (h) set to 0.14m giving an aspect ratio (b/h) of 5. The bed surface was smoothed and covered by a thin layer of concrete. The flume had a fixed bed slope of 0.001 and the error in the geometry was controlled to within 5%. A summary of experimental conditions is shown in Table 1.

Table 1 Experimental conditions

Total width (m)	Meander belt width(m)	Wavelength (m)	Inner radius (m)	Outer radius (m)	Cross-over length (m)	Side slope	valley slope	sinuosity
4.0	2.989	5.53	0.9	1.6	1.2	90°	0.001	1.381

Series name	Main channel aspect ratio (b/h)	Manning roughness n	Discharge (m^3/s)	Flow depth (m)	Bankfull depth (m)	Relative flow depth (Dr)
MN1	5	0.015	0.189	0.255	0.14	0.451
MN2	5	0.015	0.113	0.216	0.14	0.352

Four and a half meanders were constructed and the test meander is pointed out in Fig.2. In the meandering main channel, 13 vertical measurement lines were arranged where the lateral interval was 0.05m from left (y=0) to right, denoted 1 to 13 in each section and shown in Fig.3. On the floodplain, the interval of each measurement line was set as 0.2m while 17 vertical lines were arranged for CS1 and CS7 and 18 for CS2 to CS6. The measurement intervals between two vertical points were arranged as 0.015m in the main channel with 0.015m and 0.01m on the floodplain for MN1 and MN2, respectively.

All experimental data were recorded under the quasi-uniform flow conditions by ensuring that the water surface slope remained parallel to the bed slope at each meander by manually adjusting the downstream tailgate. When the deviation of water surface and bed slope became less than 5%, the quasi-uniform flow condition was considered to have been attained and the measurements were started. Using the velocity experimental data, the measurement discharges for both cases were back calculated and their errors were found to be 2.85% and 3.49%, respectively. In this paper, the lateral depth-averaged velocity distribution is modeled only along half a meander because the presence of the flow structure is periodical.

Fig.1 Photograph of the meandering compound channel in SKLH (the co-ordinate systems in the meandering main channel and on the floodplain are different, except at the apex section)
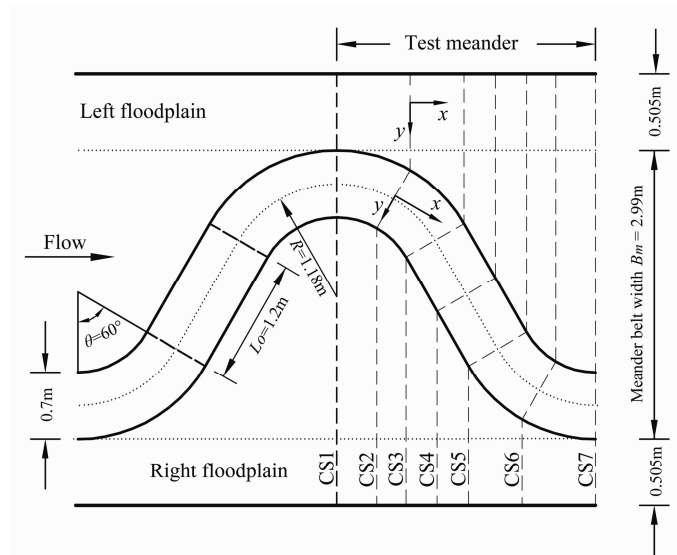
Fig.2 Plan details of geometry and measurement sections for the meandering compound channel

with the co-ordinate systems in the main channel and on the floodplain
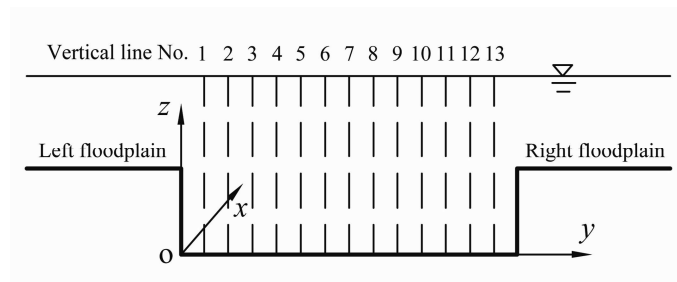
Fig.3 Measurement vertical lines in the meandering main channel

3. Region divided theory

Knight et al. [17] suggested that more accurate results can be obtained by using more divided

panels in lateral distribution methods (LDM), because of the complex secondary flow distribution

in the single channel. In this paper, the proposed model is also a two-dimensional LDM method

(outlined in Section 4) applied in a meandering compound channel and therefore, each of the

seven test sections (CS1 to CS7) is divided into several panels to obtain accurate lateral

depth-averaged velocity distributions along a meander. The research by Shiono and Muto [32] has

shown that the flow behavior is complex and strong momentum exchange exists in the vicinity of

interfaces between the main channel and floodplains, therefore, the mixing regions have to be

separated out. On the floodplain, the inside floodplain and the outside floodplain should be treated

separately, because the effect of the meandering main channel flow to the flow out of the meander

belt may be ignored (Greenhill and Sellin [7]). Finally, the main channel and two floodplains must

be separated because of the flow depth discontinuity and the divided regions in half a meander are

shown in Fig.4. In conclusion, the whole sections of CS1 and CS7 are divided into 7 panels while

that of CS2 to CS6 are divided into 9 panels.
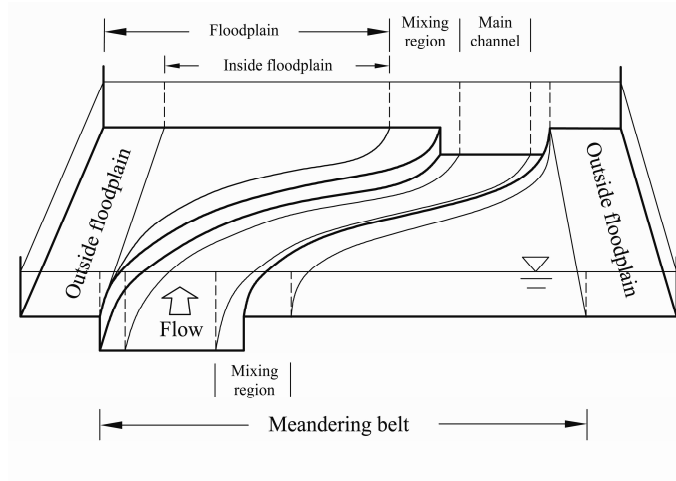
Fig.4 The scheme of divided region in the meandering compound channel

4. Theoretical background

The streamwise momentum equation for the quasi-uniform flow may be expressed as follows

$$\frac{\partial \tau_{yx}}{\partial y} + \frac{\partial \tau_{zx}}{\partial z} + \rho g S = \rho \left(U \frac{\partial U}{\partial x} + V \frac{\partial U}{\partial y} + W \frac{\partial U}{\partial z} \right) \qquad (1)$$

where x, y, z are the streamwise, lateral and vertical directions, respectively, and the co-ordinate

systems in the main channel and on the floodplain are as shown in Fig.1; τ_{yx} and τ_{zx} are the

Reynolds stresses on the planes perpendicular to y and z, respectively; ρ is the flow density; g is

the local gravitational acceleration; S is the valley slope; U, V, W are the velocity components corresponding to $\{x, y, z\}$ directions.

For an incompressible fluid, combining Eq.(1) with the flow continuity equation gives

$$\frac{\partial \tau_{yx}}{\partial y} + \frac{\partial \tau_{zx}}{\partial z} + \rho g S = \rho \frac{\partial U^2}{\partial x} + \rho \frac{\partial UV}{\partial y} + \rho \frac{\partial UW}{\partial z} \tag{2}$$

For the velocity term located on the right hand of Eq.(2), Shiono and Knight [31], Rameshwaran and Shiono [29], Huai et al. [10], Hu et al. [8], Liu et al. [20] and Yang et al. [44] ignored the streamwise velocity variation ($\frac{\partial U^2}{\partial x} \approx 0$) in a straight compound channel. However, for the meandering compound channel flow, the streamwise velocity variation must be considered due to the complex 3D flow behavior (Shiono and Muto [32], Wormleaton et al. [42] and Shiono et al. [35]). Therefore, in the analysis below, the streamwise velocity variation is included for the curved compound channel in contrast to other research (Ervine et al. [6], McGahey et al. [23] and Huai et al. [10]) where it was ignored. Further the secondary flow term ($\rho \frac{\partial UV}{\partial y}$) is reconsidered because the secondary flow is enhanced by the centrifugal force and the floodplain flow, especially at the cross-over sections.

Using the experimental data, the ratio of transverse velocity to streamwise velocity (V/U) at the centerlines of meandering main channel and outside floodplain is shown in Fig.5. From the figure, -0.04<V/U<0.04 at the center of left outside floodplain, whose intensity of secondary flow is almost the same as that in the straight channel, while -0.6<V/U<3.0 at the centerline of the meandering main channel is much larger. Apparently, the transverse velocity is enhanced significantly in the meandering main channel. Therefore, the generation mechanism of secondary

flows in the curved channel must be analyzed.
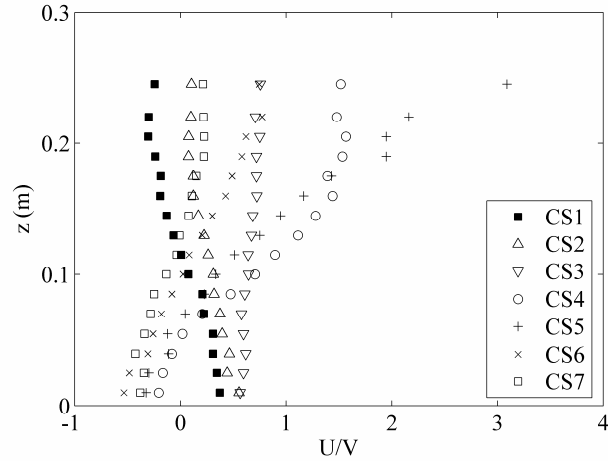
(a) the centerline of meandering main channel
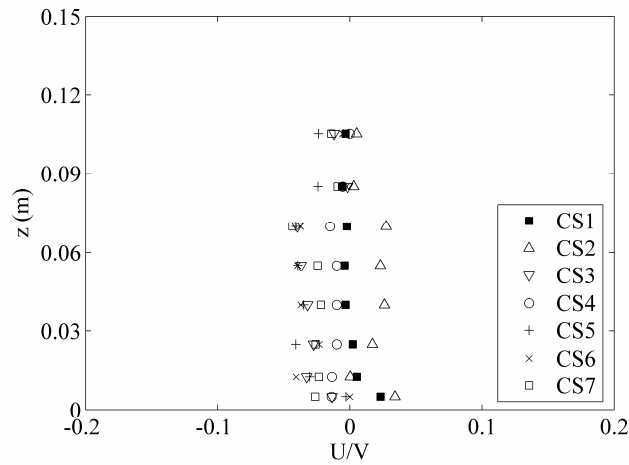
(b) the centerline of left floodplain

Fig.5 The ratio of transverse velocity to streamwise velocity ($\frac{V}{U}$), based on the experimental data

of case MN1, H=0.255m, Q=0.189m^3/s

The centrifugal force mainly contributes to the super elevation and the transverse velocity V. The

proposed model in this paper is a two-dimensional method whose governing equation is integrated

over flow height. According to research by Ervine et al. [6], Shiono and Muto [32], Shiono et

al.[33,35,36,37] and Spooner [38], the flow depth is regarded as a lateral constant by checking the

12

flow depth at every apex section as done here. Therefore, in this analytical model the lateral flow

height is assumed as a constant by ignoring the local super elevation in the main channel and the

mixing region. With regard to the influence of centrifugal force, the transverse velocity V in the

main channel increases significantly and accordingly the UV value increases as well, as seen in

Fig.6. According to dimensional analysis, the centrifugal force and the gradient of original

secondary flows have the same dimension. Hence, a direct proportion which represents the impact

extent of centrifugal force may be presented for a unit volume of water body in the meandering

main channel.

$$F_c \propto \rho \frac{\partial (UV_1)}{\partial y} \tag{3}$$

where V_1 is the transverse velocity without the effect of centrifugal force.
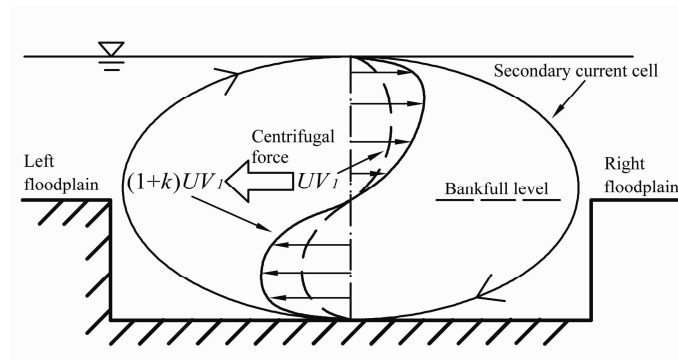
Fig.6 Effect of centrifugal force to the product of streamwise and transverse velocities at CS2

The generation of secondary flows in the meandering main channel is mainly controlled by the

centrifugal force and the lateral component of floodplain flow, especially at the cross-over sections

with large angle (θ shown in Fig.2) where the component of floodplain flow contributes

significantly. The schematic diagram of the transverse velocities at points A (CS2) and B (CS6) in

the meandering main channel is shown in Fig.7. The transverse velocity distributions are very

13

different due to the converse rotational directions of secondary flows at the points A and B. The

intensity of the secondary current above the bankfull level at CS6 is larger than that at CS2

because the secondary flow is enhanced by the component of floodplain flow when their flow

directions are the same.
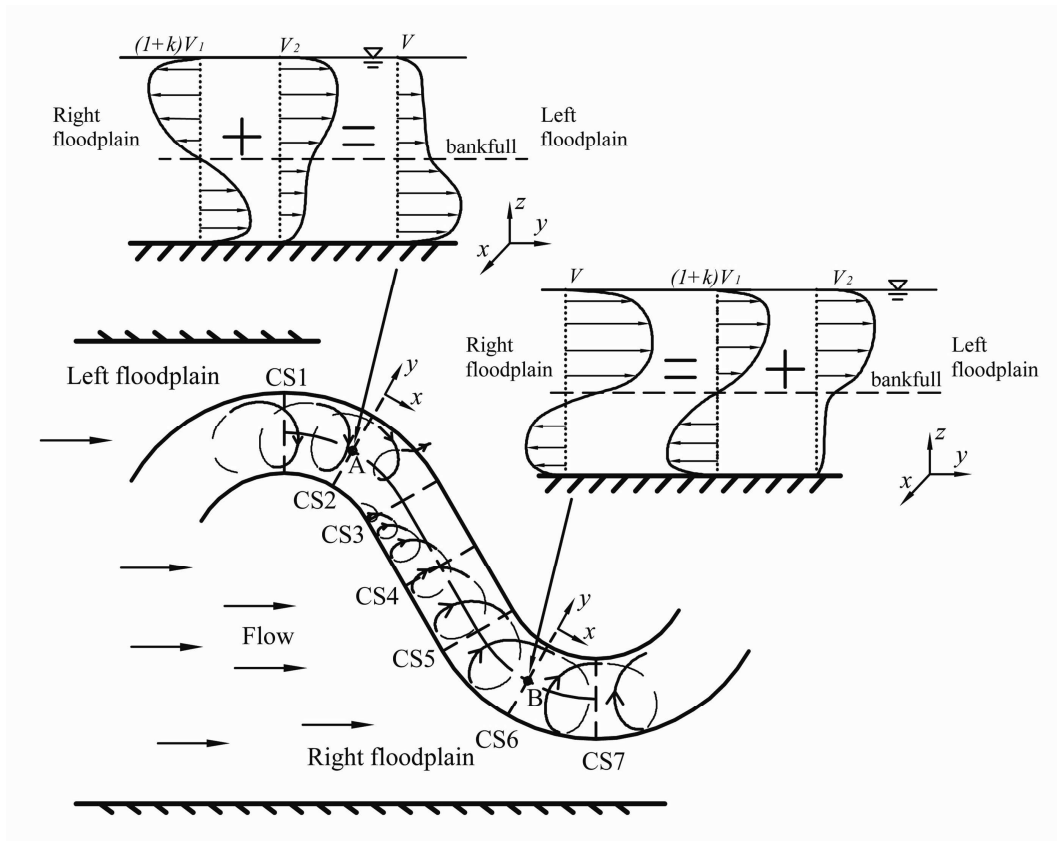
Fig.7 Vertical distributions of transverse velocities at CS2 and CS6

Based on the experimental data (case MN1) shown in Fig.8, it can be observed that the transverse

velocity (V) consists of the secondary current cell (red line), enhanced by the centrifugal force

(F_c), and the component of floodplain flow (V_2) (blue line). Therefore, the effect of centrifugal

force is assumed as $\rho k \dfrac{\partial (UV_1)}{\partial y}$, where k is a dimensionless coefficient reflecting the relation

with F_c, and which should be added into Eq.(2). The assumption made here may be most helpful

for understanding the effect of centrifugal force on original secondary flows, and this influence could be reflected by a dimensionless coefficient k in the velocity term of governing equation. Hence, Eq.(2) may be rewritten by considering the influence of centrifugal force and the component of floodplain flow as follows

$$\frac{\partial \tau_{yx}}{\partial y}+\frac{\partial \tau_{zx}}{\partial z}+\rho gS = \rho \frac{\partial U^2}{\partial x}+\rho(1+k)\frac{\partial UV_1}{\partial y}+\rho \frac{\partial UV_2}{\partial y}+\rho \frac{\partial UW}{\partial z} \tag{4}$$

where V_2 is the lateral component of the floodplain flow in the main channel, and $V = (1+k)V_1 + V_2$.

From the analysis above, it can be seen that the secondary flows at different sections along a meander vary. Some new findings about the secondary current cells in the meandering main channel are obtained (shown in Fig.8). For the apex sections (CS1 and CS7), only two secondary current cells (a large one and a small one) rotate conversely in the whole main channel while the component of floodplain flow can be ignored because the angle between the streamwise direction and flow direction is almost $0°$. For CS2 and CS6, the secondary current and the floodplain flow contribute together, and the vertical distributions of transverse velocities are changed significantly which is demonstrated by the proposed theory in Fig.7. For CS3, CS4 and CS5, the floodplain flow dominates the transverse velocity and a new secondary current cell generated from the edge of the right wall is compressed below the bankfull level (h). The new secondary current cell is first observed at CS3, and then grows rapidly from CS4 to CS6, reaching its largest at CS7. The periodic phenomenon can also be discovered in the previous meander and the subsequent one, therefore, the observed converse rotation of secondary current cells at CS1 may be explained clearly.
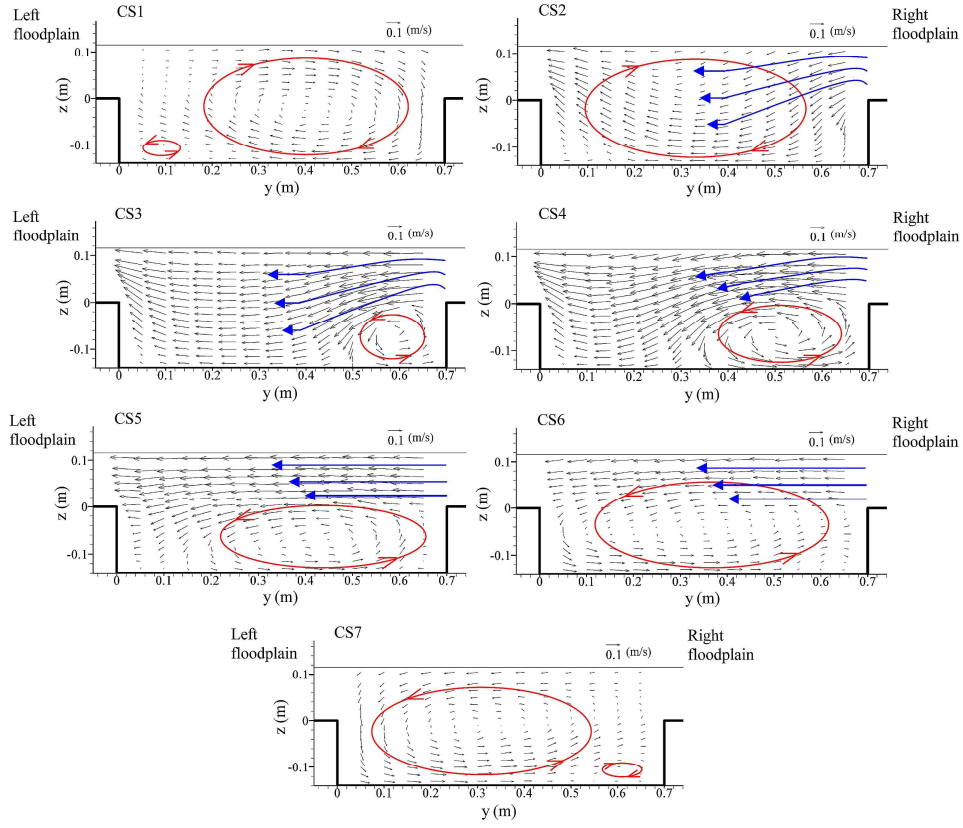
Fig.8 Generation mechanism of secondary flows in the meandering main channel, based on the

experimental data of case MN1, H=0.255m, Q=0.189m^3/s

Integrating Eq.(4) over the flow height (H) gives different results at various sections

$$\frac{\partial}{\partial y}\left(\rho\lambda H^2\sqrt{\frac{f}{8}}U_d\frac{\partial U_d}{\partial y}\right)-\rho\frac{f}{8}U_d^2+\rho gS=K \tag{5}$$

and $U_d=\frac{1}{H}\int_0^H Udz$; $\tau_b=\rho\left(\frac{f}{8}\right)U_d^2$; $\overline{\tau}_{yx}=\rho\overline{\varepsilon}_{yx}\frac{\partial U_d}{\partial y}$; $\overline{\varepsilon}_{yx}=\lambda HU_*$ $\qquad$ (6)

where λ is the dimensionless eddy viscosity; f is the Darcy-Weisbach friction factor; U_d is the

depth-averaged velocity; K is the velocity variation parameter whose expression depends on the

test sections, shown in Eqs.(7)-(9); τ_b is the bed shear stress; $\overline{\tau}_{yx}$ is the depth-averaged

Reynolds shear stress; $\overline{\varepsilon}_{yx}$ is the depth-averaged eddy viscosity; U^* is the shear velocity

$(=\sqrt{\frac{f}{8}}U_d)$.

16

From the analysis of secondary flows in the main channel, the transverse velocity (V) is seen to consist of V_1 and V_2 whose effects are different at each section, which in turn leads to various expressions for K. Therefore,

For apex sections (CS1 and CS7), $\quad K = \rho H \dfrac{\partial U_d^{\,2}}{\partial x} + \rho(1+k)H \dfrac{\partial (UV_1)_d}{\partial y}$ (7)

For cross-over sections (CS2 and CS6), $K = \rho H \dfrac{\partial U_d^{\,2}}{\partial x} + \rho(1+k)H \dfrac{\partial (UV_1)_d}{\partial y} + \rho H \dfrac{\partial (UV_2)_d}{\partial y}$ (8)

For cross-over sections (CS3, CS4 and CS5), $\quad K = \rho H \dfrac{\partial U_d^{\,2}}{\partial x} + \rho(1+k)h \dfrac{\partial (UV_1)_d}{\partial y} + \rho H \dfrac{\partial (UV_2)_d}{\partial y}$ (9)

In order to simplify Eq.(5), simple expressions are derived for the streamwise variation of $U_d^{\,2}$ and the lateral variation of $(UV)_d$ as follows

$$K_x = \frac{\partial U_d^{\,2}}{\partial x}, \quad K_{y1} = \frac{\partial (UV_1)_d}{\partial y} \quad \text{and} \quad K_{y2} = \frac{\partial (UV_2)_d}{\partial y} \tag{10}$$

Where K_x is the streamwise variation coefficient; K_{y1} and K_{y2} are the secondary flow coefficients ($K_y = K_{y1} + K_{y2}$). It should be noted that the coefficients of Eq.(10) are not constant in the streamwise and lateral directions and in order to present the analytical solutions of Eq.(5), they are assumed as constants in each divided panel. Therefore, the velocity term in the meandering main channel may be rewritten as

For apex sections (CS1 and CS7), $\quad K = \rho H K_x + \rho(1+k)H K_{y1(H)}$; (11)

For cross-over sections (CS2 and CS6), $\quad K = \rho H K_x + \rho(1+k)H K_{y1(H)} + \rho H K_{y2(H)}$; (12)

For cross-over sections (CS3, CS4 and CS5), $\quad K = \rho H K_x + \rho(1+k)h K_{y1(h)} + \rho H K_{y2(H)}$; (13)

where the subscripts "H" and "h" are the flow height and the bankfull height, respectively. Due to the different integral heights, the subscript is shown herein to avoid misunderstanding.

On the floodplain, the velocity term without the effect of centrifugal force may be simplified as

$$K = \rho(H-h)K_x + \rho(H-h)K_{y(H-h)} \tag{14}$$

The analytical solution of Equation (5) is shown as

$$U_d = \sqrt{A_1 e^{\gamma_1 y} + A_2 e^{\gamma_2 y} + \omega} \tag{15}$$

where $\gamma_1 = \dfrac{1}{H}\left(\dfrac{2}{\lambda}\right)^{1/2}\left(\dfrac{f}{8}\right)^{1/4}$; $\gamma_1 = -\gamma_2$; $\omega = \dfrac{8gHS}{f}\left[1 - \dfrac{K}{\rho gHS}\right]$, A_1 and A_2 are unknown constants.

5. Boundary conditions

To obtain the analytical solutions for U_d [Eq.(15)] the unknown constants need to be eliminated by appropriate boundary conditions. For the apex sections (CS1 and CS7), the boundary conditions are easily established because the co-ordinate system on the floodplain is coincident with that in the meandering main channel. However, the boundary condition should be reconsidered for the cross-over sections (CS2 to CS6) where the co-ordinate systems of main channel and floodplains include an angle (θ) (θ =30°for CS2 and CS6; θ =60°for CS3, CS4 and CS5).

The planforms of depth-averaged velocity for MN1 and MN2 in half a meander are shown in Fig.9, and it is noticeable that the true flow directions in the main channel do not follow the valley direction. This phenomenon was also observed by Shiono et al. [36] and can be attributed to the influence of centrifugal force and floodplain flow, especially at the cross-over sections (CS2 to CS6) with overbank flows. The relation of the velocities in the main channel and on the floodplain is shown in Fig.10, where $U_{d(1)}$ is the depth-averaged velocity on the floodplain, $U_{d(2)}$ is the projection of $U_{d(3)}$ in the streamwise direction on the floodplain, $U_{d(3)}$ is the depth-averaged velocity in the main channel with the true flow direction, and $U_{d(4)}$ is the measured experimental

depth-averaged velocity following the valley direction in the main channel.
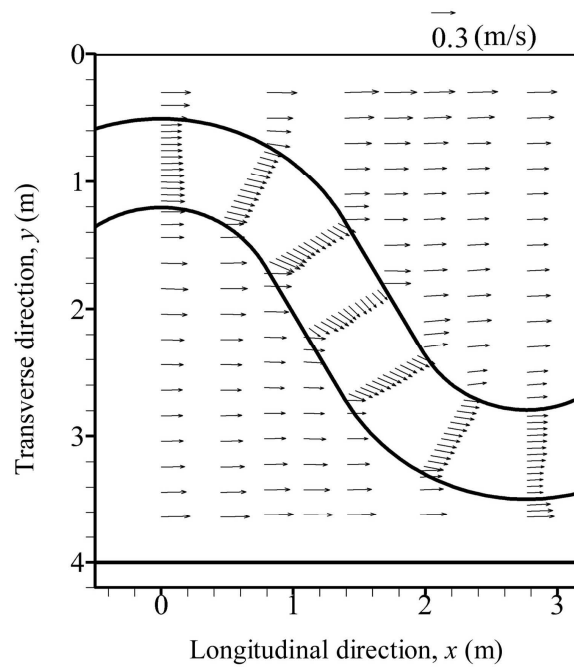
(a) case MN1
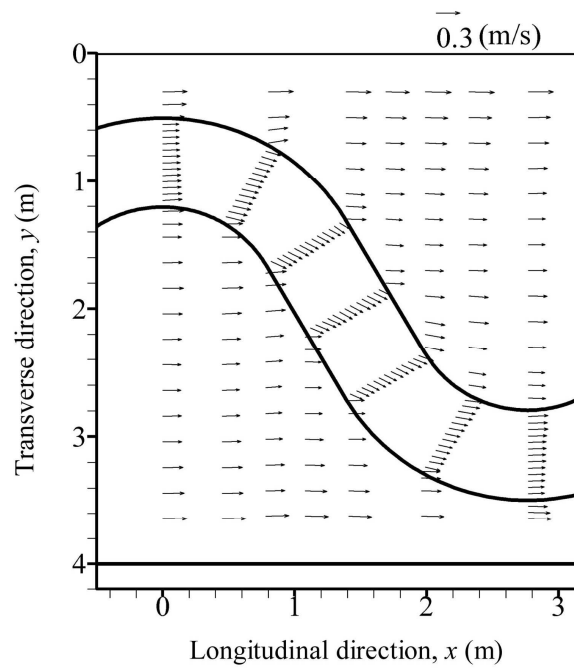
(b) case MN2

Fig.9 Planform of depth-averaged velocity along half a meander for two cases

When points A and C are infinitely close to point B (i.e. $\Delta Y \to 0$ and $\Delta L \to 0$), the velocity at

point A equals that at the point C:

$$U_{d(1)} = U_{d(2)} \tag{16}$$

Due to the relation of velocities shown in Fig.10, the three velocities ($U_{d(2)}$, $U_{d(3)}$ and $U_{d(4)}$) at

the point C in the main channel may be inter-changed.

$$U_{d(2)} = \frac{U_{d(3)}}{\cos\theta_2} = \frac{U_{d(4)}}{\cos\theta_1 \cos\theta_2} \tag{17}$$

where θ_1 is the angle between $U_{d(3)}$ and $U_{d(4)}$; θ_2 is the angle between $U_{d(2)}$ and $U_{d(3)}$;

$\theta = \theta_1 + \theta_2$.
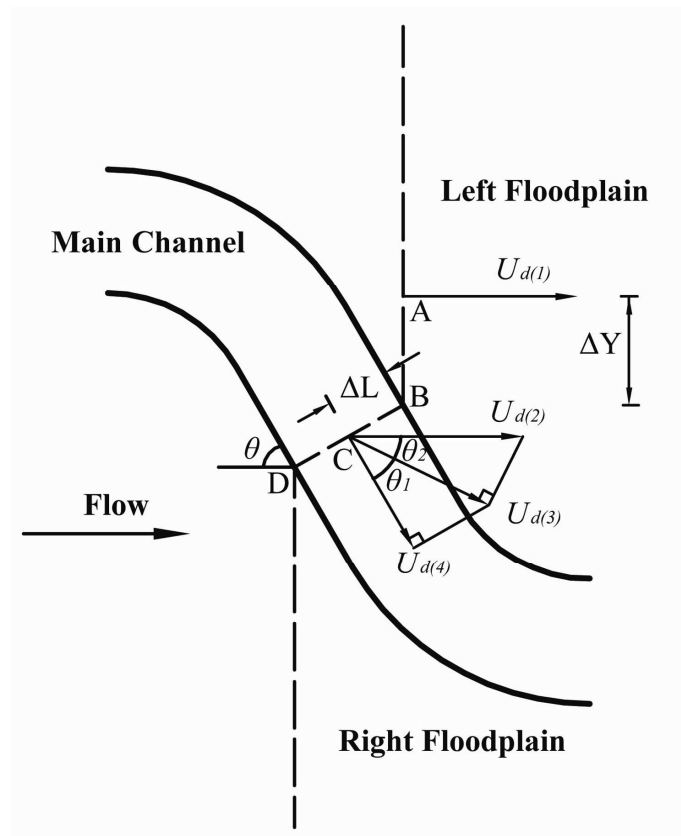
Fig.10 Relation of depth-averaged velocities and the angles in the main channel and on the

floodplain

For the cases MN1 and MN2, we derived the lateral distributions of θ_1 from CS1 to CS7 from the experimental data, shown in Fig.11. From the figure, the θ_1 values at CS1 and CS7 are almost equal to $0°$, θ_1 values ranges between $12.6°$ and $24.2°$ at CS2 and CS6 while $\theta_1 = 23.3° \sim 37.0°$ is observed at CS3, CS4 and CS5. Therefore, the assumption of $\theta_1 = \theta_2 = \dfrac{\theta}{2}$ is made at each section for cases MN1 and MN2, leaving $\theta_1 = \theta_2 = 0°$ at CS1 and CS7, $\theta_1 = \theta_2 = 15°$ at CS2 and CS6, and $\theta_1 = \theta_2 = 30°$ at CS3, CS4 and CS5, which almost equals the mean values of the experimental data. Therefore, the velocity continuity and velocity gradient continuity at the interfaces of main channel and floodplains have to contain θ_1 and θ_2, and new boundary conditions are as follows:

- No-slip condition, i.e. $U_d = 0$ at remote boundary;

- Continuity of velocity at each domain junction, i.e. $U_d^{(i)} = \dfrac{U_d^{(i+1)}}{\cos\theta_1 \cos\theta_2}$;

- Gradient continuity of velocity at each domain junction, i.e. $\dfrac{\partial U_d^{(i)}}{\partial y} = \dfrac{1}{\cos\theta_1 \cos\theta_2} \dfrac{\partial U_d^{(i+1)}}{\partial y}$.

where the superscript (i) is the number of divided panels.

Noting $\theta_1 = \theta_2 = 0°$ at the interfaces of divided panels on the floodplain, therefore, the continuity of velocity and velocity gradient are simplified as $U_d^{(i)} = U_d^{(i+1)}$ and $\dfrac{\partial U_d^{(i)}}{\partial y} = \dfrac{\partial U_d^{(i+1)}}{\partial y}$.
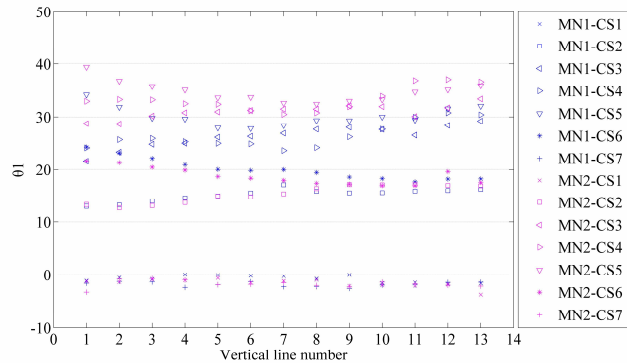
Fig.11 The lateral distribution of the angle θ_1 in the meandering main channel at CS1 to CS7

(*H*=0.255m for case MN1 and *H*=0.216 for case MN2)

6. Determination of model parameters

Applying this approach to model the depth-averaged velocity, all parameters remain constant in each divided panel. Before applying this model, four coefficients, i.e. Darcy-Weisbach friction factor (f), dimensionless eddy viscosity (λ), velocity parameter (K), need to be determined as follows.

The Darcy-Weisbach friction factor (f) is usually back calculated by the experimental data from depth-averaged velocity and bed shear stress (Shiono and Knight [31], Tang and Knight [40]). Because there is no means for measuring the boundary shear stress, the expression $f = \dfrac{8gn^2}{R^{1/3}}$, proposed by Knight et al. [17] and Huai et al. [9] was used to predict the Darcy-Weisbach friction factor (f) in the main channel and the floodplains.

For the dimensionless eddy viscosity (λ), in a straight compound channel, Shiono and Knight [31] illustrated that λ changed slightly in the main channel and significantly on the floodplain. Later, a practical relationship for $\lambda_{fp} = \lambda_{mc}(1.2Dr^{-1.44} - 0.2)$ was presented by Abril and Knight [1] to predict λ_{fp} on the floodplain, where *Dr* is the relative depth defined as (*H-h*)/*H*, and the subscripts "*mc*" and "*fp*" refer to the main channel and the floodplain, respectively. However, based on the experimental data (shown in Table 2) in the meandering compound channel, the dimensionless eddy viscosity (λ_{mc}) changes along a meander, and it is noticeable that the λ_{mc} values at the apex sections of main channel are almost 0.07 which are the same as those in the straight compound channel while λ_{mc} values at the cross-over sections are about half of 0.07. The mean values of

λ_{mc} at CS2 to CS6 for MN1 and MN2 are 0.038 and 0.045, respectively. On the floodplain, the

mean values of λ_{fp} are 0.132 and 0.121 for MN1 and MN2, respectively, where the predictive

relation proposed in the straight compound channel by Abril and Knight (2004) cannot estimate

the λ_{fp} accurately.

Table 2 Dimensionless eddy viscosity at each section

Case		CS1	CS2	CS3	CS4	CS5	CS6	CS7
MN1	λ_{mc}	0.075	0.033	0.036	0.032	0.038	0.049	0.070
	λ_{fp}	0.145	0.135	0.101	0.140	0.117	0.148	0.137
MN2	λ_{mc}	0.069	0.042	0.040	0.043	0.050	0.049	0.068
	λ_{fp}	0.127	0.117	0.101	0.122	0.119	0.141	0.123

Finally, Eqs.(7)-(9) define the velocity variation parameter (K) at the apex and cross-over sections

due to the different generation mechanisms of secondary flows. These equations may be used to

calculate K in CS1~7 if detailed experimental velocities are available. K values apparently change

along half a meander because the strength of secondary flows in the main channel and the effect of

floodplain flow are different. Since lateral variation of secondary flows and longitudinal variation

of velocity cannot be easily described at different cross-sections, velocity variation parameters (K)

are back calculated at all the seven sections by Eq.(5) which are shown in Figs.12 and 13. From

the figures, it is apparent that the velocity parameter is a lateral variable, hence, the determination

of velocity parameter (K) is not straightforward. In this model, the differing ranges are determined

by the experimental data, which are 1.4~1.8 and 1.2~1.5 in the meandering main channel for MN1

and MN2, respectively. On the floodplain, the K values range within 0.22~1.25 and 0.21~0.78 for

MN1 and MN2, respectively. These ranges may provide the references for choosing the most

suitable K value in each divided region. Therefore, the velocity parameter (K) is selected as a

constant in each panel among the experimentally determined ranges and is slightly modified as a calibration parameter until the best results are obtained. If only depth-averaged velocities are known, the velocity parameter is empirically calibrated in order to give best fit with the experimental velocities. In different channels, the proposed model is still useful in identifying key processes and demonstrating their importance and once the velocity parameter has been calibrated for each case it can predict results at other depths for the same geometry. This methodology is also applicable in the natural river with much higher Manning coefficient due to the mobile bed and flood plain vegetation if the complex cross-sectional shape can be simplified as a regular form.
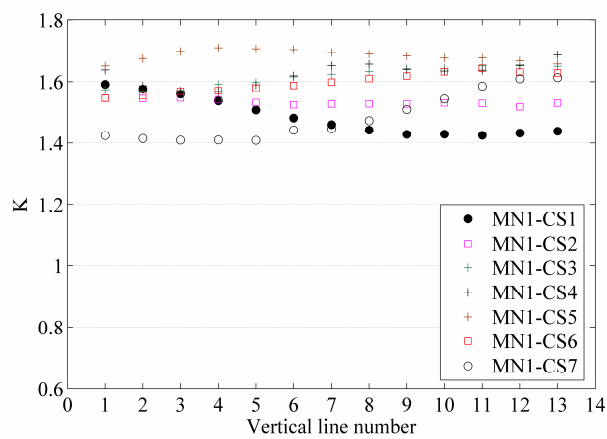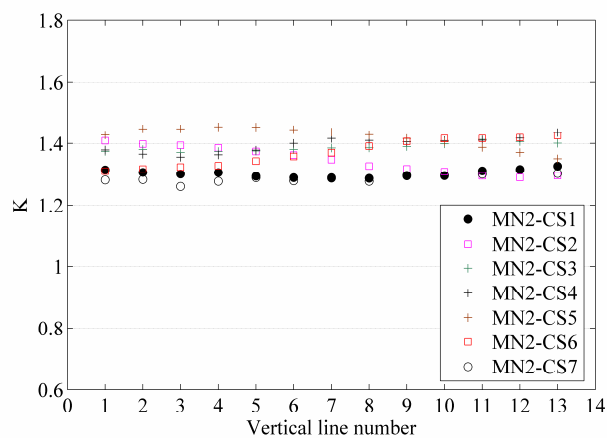
(a) case MN1, H=0.255m, Q=0.189 m^3/s

Fig.12 Lateral distributions of velocity variation parameter K in the meandering main channel at
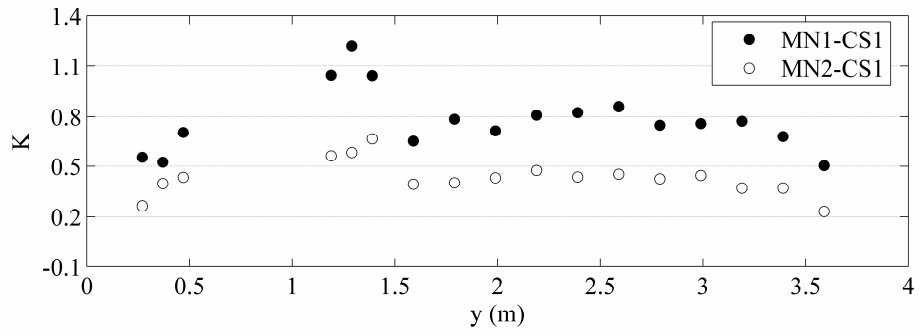
CS1 to CS7

(a)CS1
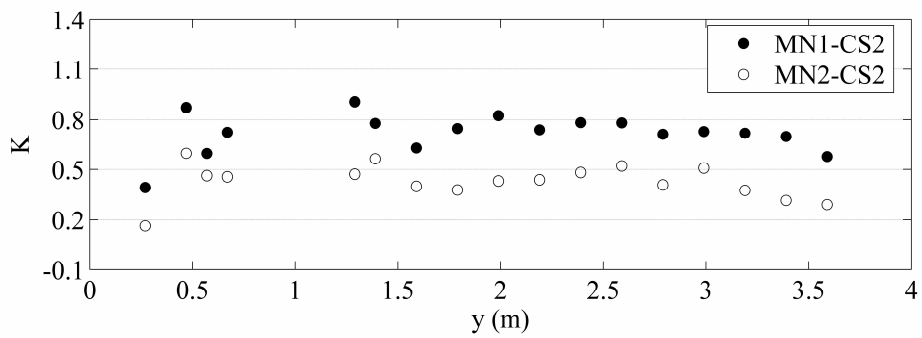
(b)CS2
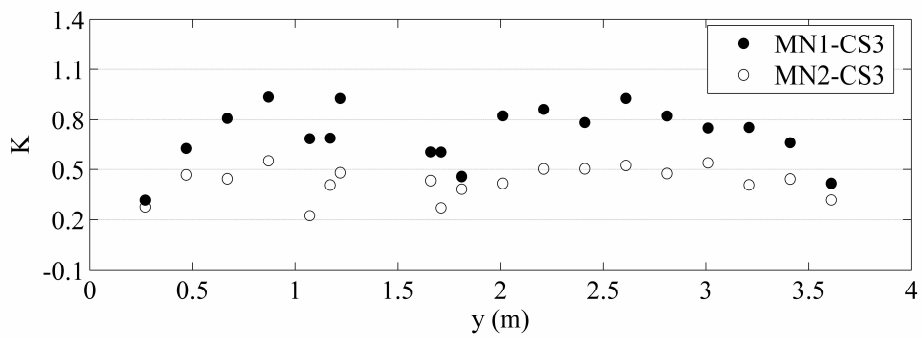
(c)CS3
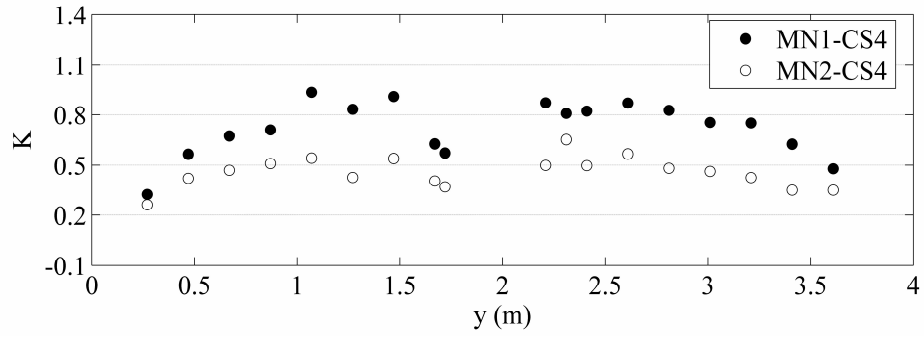
(d)CS4
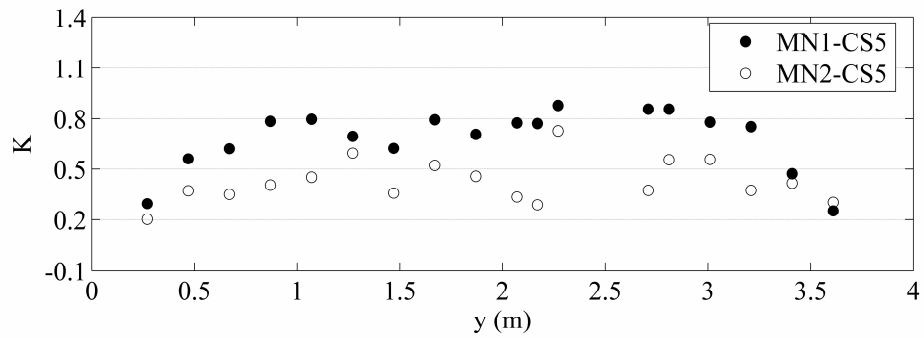
(e)CS5
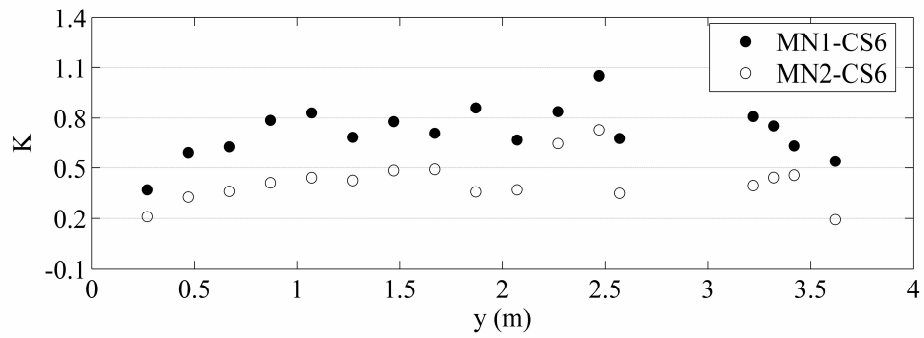
(f)CS6
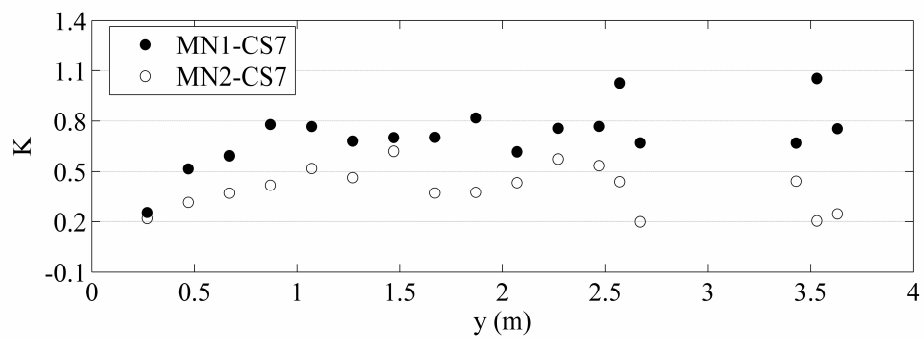
(g)CS7

Fig.13 Lateral distributions of velocity variation parameter K on the floodplain at CS1 to CS7

7. Application

In order to plot all the modeling results and experimental data in one figure, the projection of lateral direction (y) in the meandering main channel is used for cross-over sections. The experimental data along half a meander have been compared with the results from the proposed method, shown in Figs.14 and 15. From these figures, the method with the slightly modified velocity variation parameters (K) in each divided panel presents accurate results from CS1 to CS7 for cases MN1 and MN2. It should be noted that the modeled lateral depth-averaged velocity distribution follows the experimental data closely at the cross-over sections, especially at the ones with large angle θ (CS3, CS4 and CS5), when using the new boundary condition described in Section 5. The poor modeling results seen when neglecting the angles [i.e. θ_1 and θ_2 in Eq.(17)] indicates that the assumption of the new boundary condition is appropriate, accurate and reliable.

The chosen velocity variation parameters (K) in each divided region are shown in Table 3. It is apparent that the K values in the meandering main channel are much larger than those on the floodplain, indicating that the centrifugal force and the overtopping flow contribute heavily. The largest K values in the three panels of the main channel appear at the left mixing region (in CS1, CS2 and CS3), then move to the center region (in CS4 and CS5), finally appearing in the right mixing region (in CS6 and CS7). On the floodplain, the K values on the inside floodplain are 0.6~0.8 and 0.4~0.5 which are almost equal to the experimental values at each section, as shown in Fig.13. Eq.(14) shows that only the streamwise variation of velocity and the lateral variation of secondary flows are considered. Therefore, the K values on the inside floodplain are much smaller when compared with the ones in the main channel. However, the K values on the outside floodplain are only 0.4 and 0.2 for MN1 and MN2, respectively, which are about half of the values

on the inside floodplain. This phenomenon may be explained by the fact that the flow on the outside floodplain is affected slightly by the flow in the meander belt, and the horizontal shear stress generated between the inbank flow and the overtopping flow would not influence the outside floodplain flow significantly. Greenhill and Sellin [7] proposed a modified Manning's Equation to predict the stage-discharge curve in the meandering compound channel and found that good results were obtained by separately considering the meander belt flow and the outside floodplain flow. Hence, the streamwise variation can be ignored on the outside floodplain, and Eq.(14) may be simplified as $K = \rho(H-h)K_{y(H-h)}$ and the K value is absolutely becoming small.

Table 3 Velocity variation parameter in each divided panel

Case	Section	Left floodplain			Main channel			Right floodplain		
		Outside floodplain	Inside floodplain	Mixing region	Left Mixing region	Center region	Right Mixing region	Mixing region	Inside floodplain	Outside floodplain
MN1	CS1	0.4	-	-	1.9	1.5	1.4	0.8	0.7	0.4
	CS2	0.4	-	0.8	1.8	1.6	1.5	0.6	0.8	0.4
	CS3	0.4	0.7	0.4	1.9	1.7	1.6	0.6	0.8	0.4
	CS4	0.4	0.7	0.7	1.6	1.8	1.6	0.8	0.8	0.4
	CS5	0.4	0.7	0.6	1.7	1.8	1.7	0.7	0.8	0.4
	CS6	0.4	0.7	0.8	1.5	1.7	1.8	0.7	-	0.4
	CS7	0.4	0.7	0.8	1.5	1.6	1.9	-	-	0.4
MN2	CS1	0.2	-	-	1.6	1.3	1.2	0.5	0.5	0.2
	CS2	0.2	-	0.45	1.5	1.4	1.3	0.4	0.5	0.2
	CS3	0.2	0.5	0.45	1.6	1.4	1.4	0.4	0.5	0.2
	CS4	0.2	0.5	0.5	1.3	1.6	1.3	0.5	0.5	0.2
	CS5	0.2	0.5	0.4	1.4	1.5	1.5	0.5	0.5	0.2
	CS6	0.2	0.5	0.5	1.3	1.4	1.5	0.5	-	0.2
	CS7	0.2	0.5	0.5	1.2	1.3	1.6	-	-	0.2

For practical engineering purposes, the lateral distributions of U_d along a meander are

sufficiently accurate and may be used to predict the stage-discharge curve by integrating U_d laterally. The discharge prediction is appropriately done at the apex cross-section where the horizontal shear stress is small (Shiono and Muto [32]). At the cross-over section with larger angle between the meandering main channel and floodplain, the stronger horizontal shear stress leads to more energy losses. Consequently, a lower local velocity distribution is predicted and a smaller discharge is obtained. When this model is applied in the natural river to predict the lateral velocity distribution at different locations, the more complex river geometries with more divided panels are really needed. The values of λ, f and K are still assumed as constants in each panel, and their variations in each panel with increasing flow stage should be reasonably systematic. The K value in the natural river will be more difficult to determine because the secondary flow distributions in a natural river are more complex than that in the experimental flume with a non-mobile bed. However, fortunately the K value is the only free parameter in this model, and good results along a meander may be obtained by modifying it in each divided panel when the lateral velocity distribution is obtained. In addition, the sediment transport rate may be also calculated using the local boundary shear stress ($\tau_b = \rho \frac{f}{8} U_d^2$) and using an appropriate transport equation.

(a) CS1

29
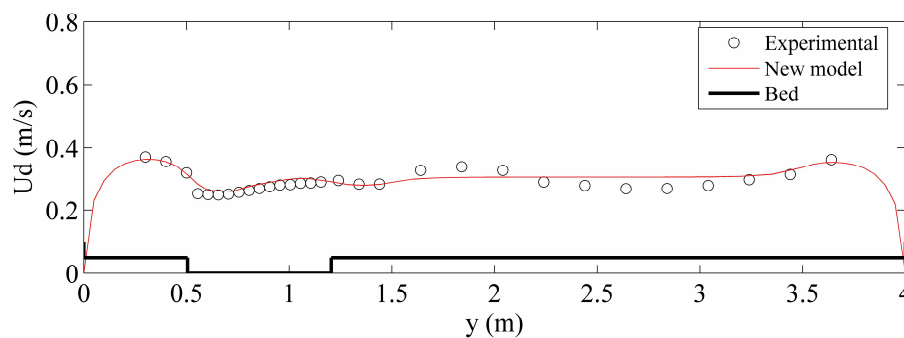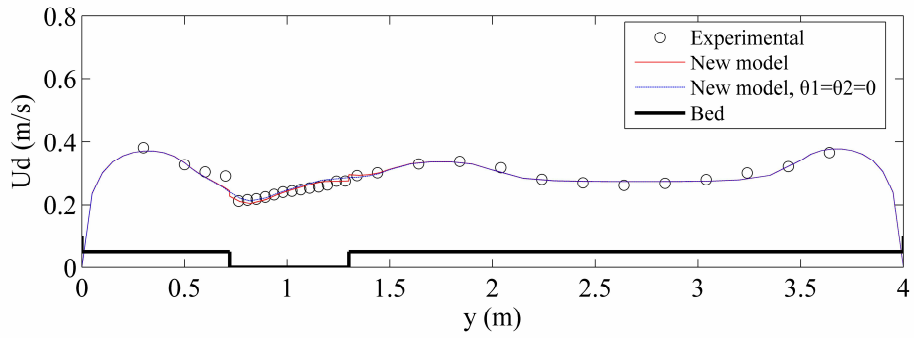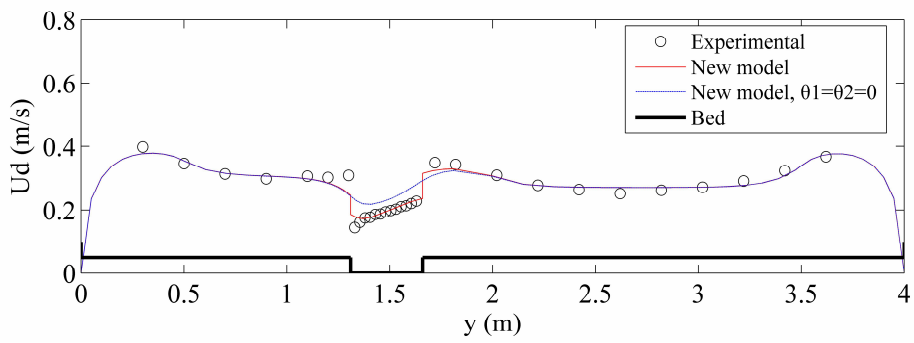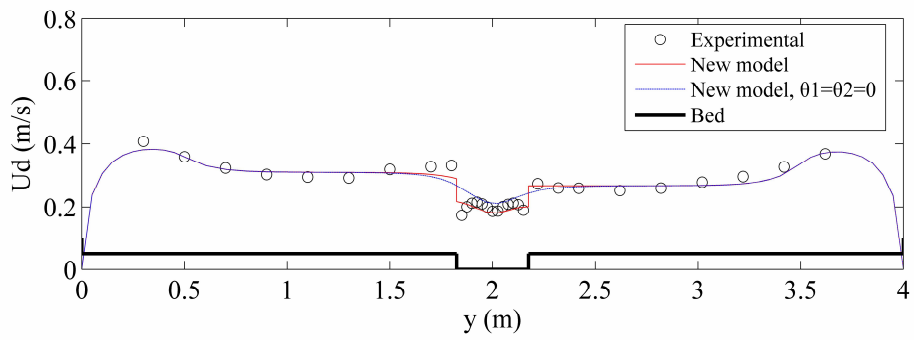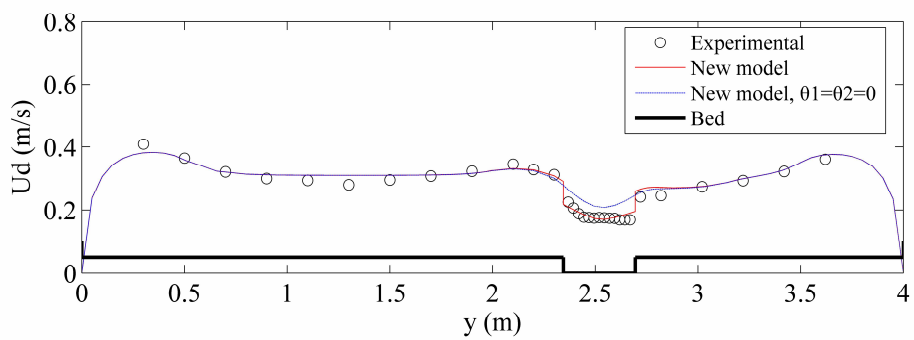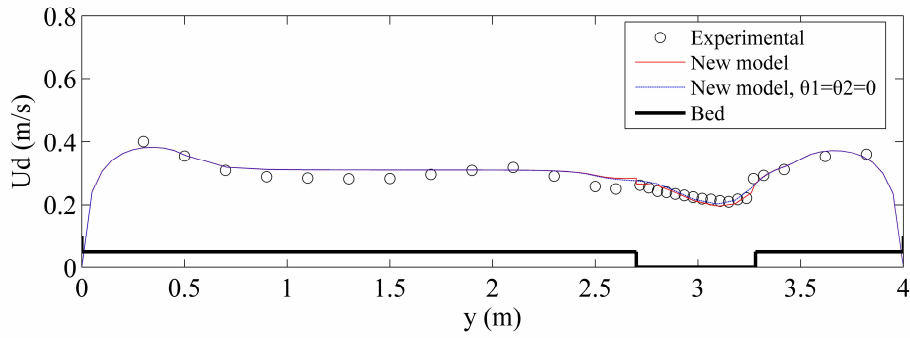
(b)CS2
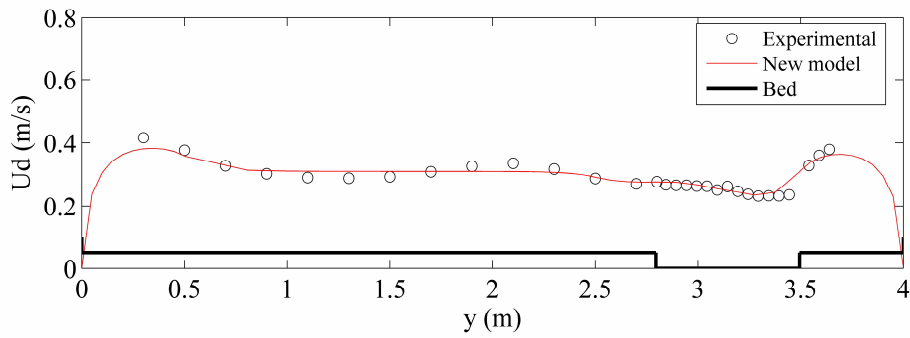
(c)CS3

(d)CS4

(e) CS5

(f) CS6

(g) CS7

Fig.14 Modeling depth-averaged velocity from CS1 to CS7 with experimental data for case MN1,

H=0.255m, Q=0.189 m^3/s
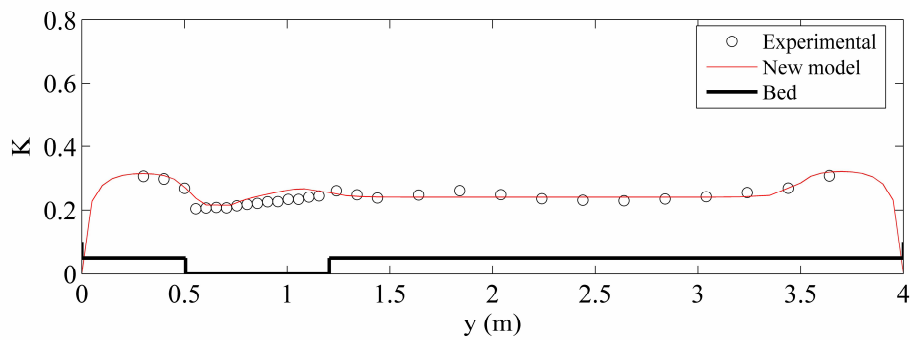
(a) CS1
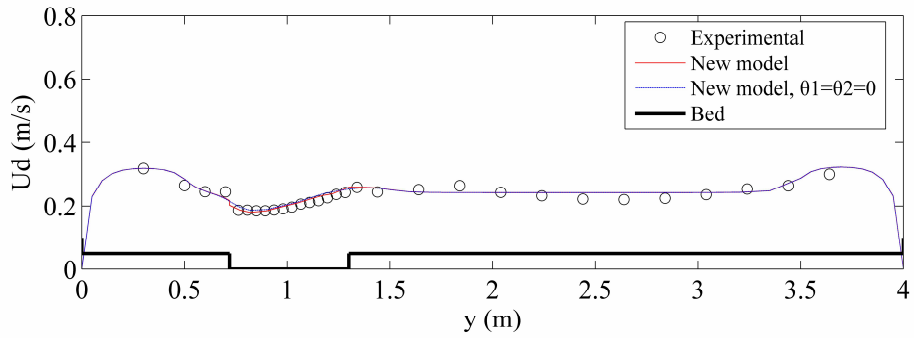
(b) CS2
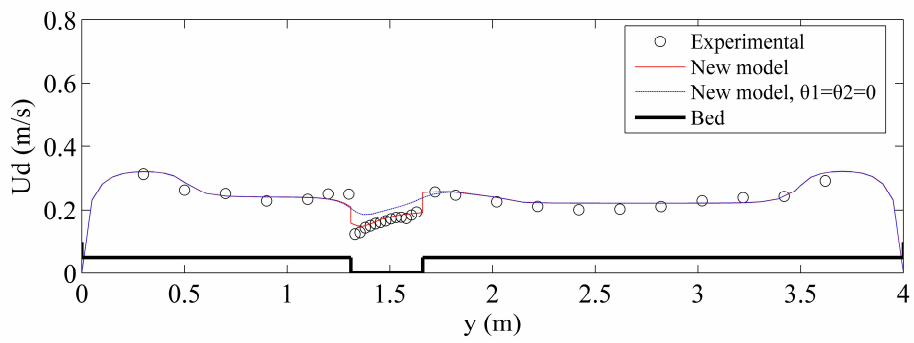
(c) CS3
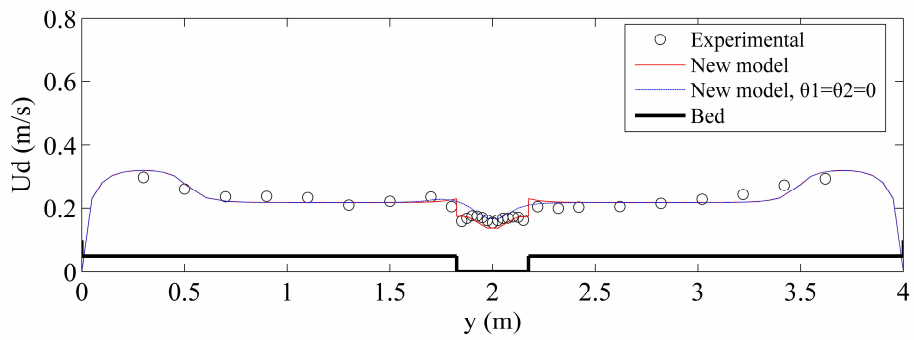
(d) CS4
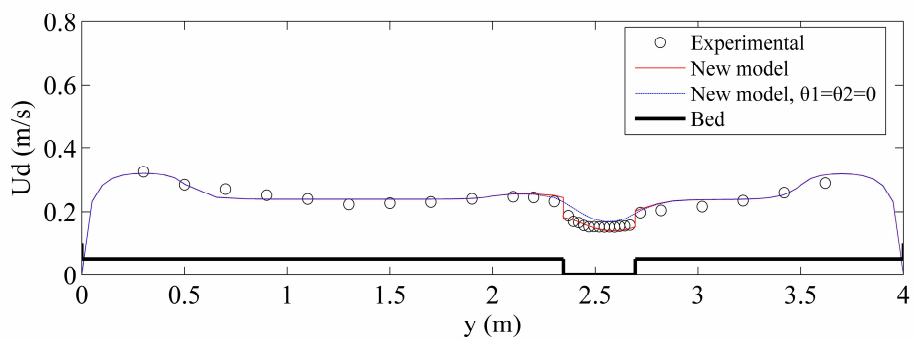
(e) CS5
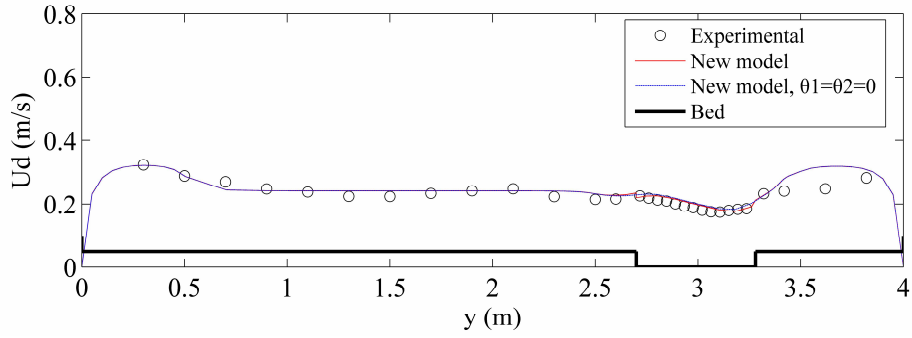
(f) CS6
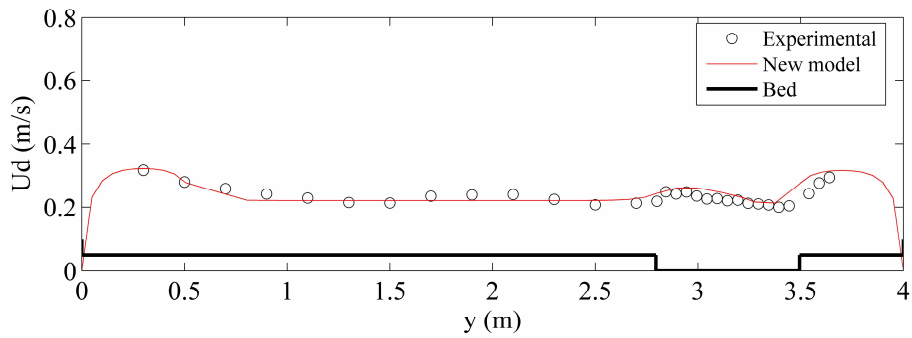
(g) CS7

Fig.15 Modeling depth-averaged velocity from CS1 to CS7 with experimental data for case MN2,

$$H = 0.216\text{m}, Q = 0.113 \text{ m}^3/\text{s}$$

8. Discussion

8.1 Components in velocity term

According to Eqs.(11)-(13), the velocity variation parameter (K) contains the streamwise variation

of velocity (K_x) and lateral variation of secondary flow (K_y) which merit further discussion. The

two parameters are back calculated from the experimental data, and K_x values at each section are

shown in Fig.16. From the figures, the variation pattern at every vertical follows a linear relation

which is different at vertical line 1 to 13. The K_x values at the vertical line 1 and 4 remain

negative at CS2 and CS3 while positive at CS4, CS5 and CS6. For the vertical line 7 and 10, the

K_x values remain negative at CS2, CS3 and CS4 and positive at CS5 and CS6. About the vertical

line 13, the K_x values are all negative except at CS6. At the apex sections (CS1 and CS7), the K_x values at all vertical lines are almost zero. From the Figs.14 and 15, the U_d values at the apex sections are the maximal values which can be used to explain the K_x values, which are the gradient of U_d^2 (Eq.(10)), at CS1 and CS7 equal 0. Therefore, the velocity term at the apex section (Eq.(7)) may be simplified as

For apex sections (CS1 and CS7), $\quad K = \rho(1+k)H\dfrac{\partial(UV_1)_d}{\partial y}$ \hfill (18)
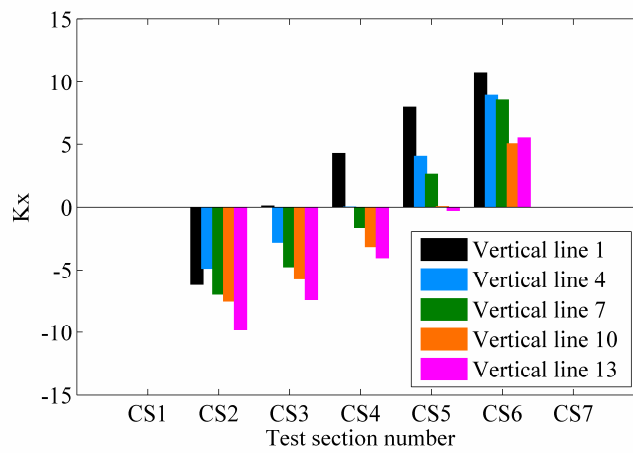
(a) MN1
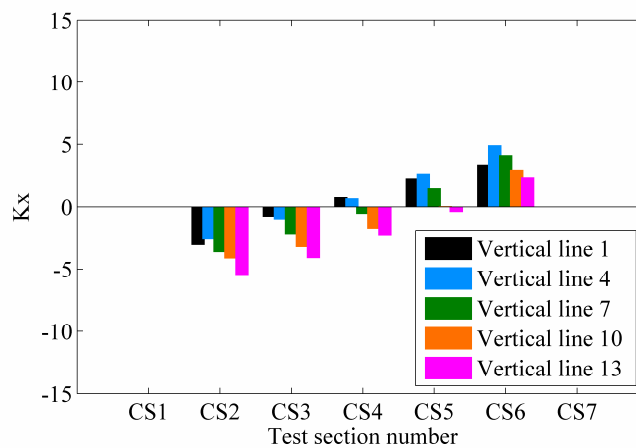
(b) MN2

Fig.16 Streamwise variation coefficient K_x in the meandering main channel at CS1 to CS7

Equation (18) demonstrates that good prediction at the apex section can be still obtained by

ignoring the streamwise velocity variation (K_x). Research by Ervine et al. [5], McGahey et al. [23] and Huai et al. [10] who ignored the streamwise velocity variation and only applied their models at the apex section in the meandering compound channel are, in fact, specific cases of the model presented here. The modified secondary parameter proposed by Ervine et al. [5] actually contained the effect of centrifugal force, demonstrated by the parameters in the meandering main channel which were much larger than those in the straight main channel in their paper. In this paper, the *K* value itself including the k defined in Eq.(3) can reflect the effect of centrifugal force in the meandering main channel, where the *K* values are larger than the ones on the floodplain (shown in Table 3).

For the secondary flows in the meandering main channel, the secondary flow variation coefficient (K_y) from CS1 to CS7 has been also calculated, and the lateral distribution is shown in Fig.17. From the figures, the K_y values at CS1 are almost equal the ones at CS7, and remain positive. This can be explained by the definition of K_y which is the lateral gradient of $(UV)_d$. The rotational directions of secondary flows at CS1 and CS7 are converse while the intensities are almost the same (see Fig.8). Therefore, the K_y values are nearly the same at the apex sections. At the cross-over sections (CS2 to CS6), the floodplain flows contribute to the secondary flow, and the K_y values at the right side seem larger because the floodplain flow plunges into the main channel from the right bank in the half test meander shown in Fig.2, leading to the stronger transverse velocity. The biggest lateral K_y values are shown at CS2, then gradually reduce and reach the lowest values at CS6.
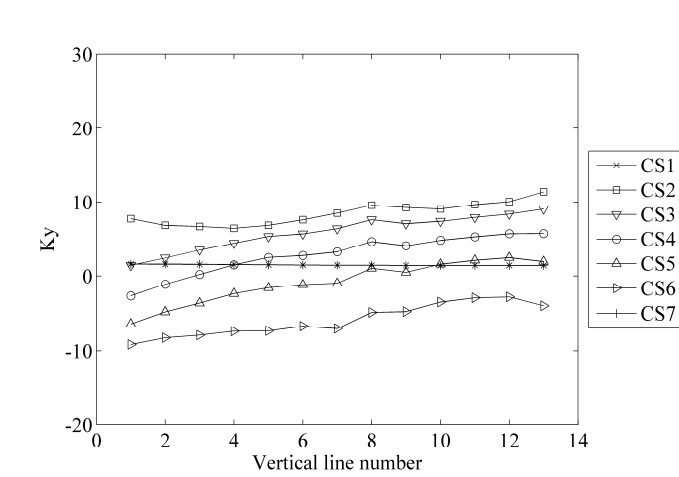
(a) MN1
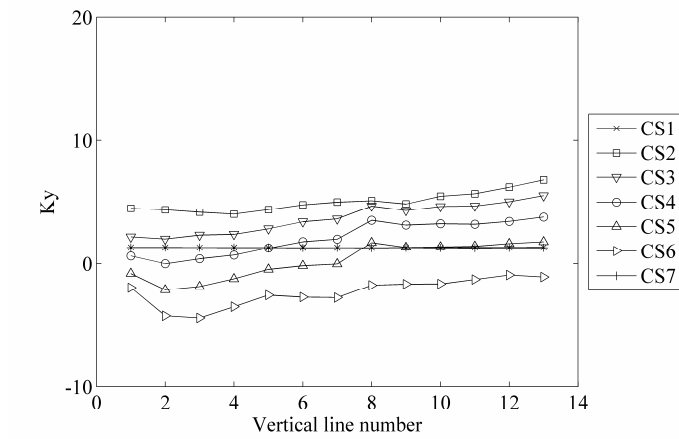
(b) MN2

Fig.17 Lateral distributions of secondary flow coefficient K_y in the meandering main channel at

CS1 to CS7

On the floodplain, the K values reduce significantly compared with the ones in the meandering main channel due to the absence of centrifugal force and floodplain flow. The ratios of $\frac{K_x}{K}$ at the centerline of the outside floodplains are shown in Fig.18. It can be clearly seen that the ratios are very small, indicating that the streamwise variation of velocity may be ignored. However, at the centerline of the inside floodplains, the $\frac{K_x}{K}$ values range between 0.2~2.1 which cannot be

ignored during the calculation, representing that the effect of main channel flow to the inside floodplain flow cannot be ignored. The analysis above explains why the K values on the outside floodplains are only a half of the ones on the inside floodplains.
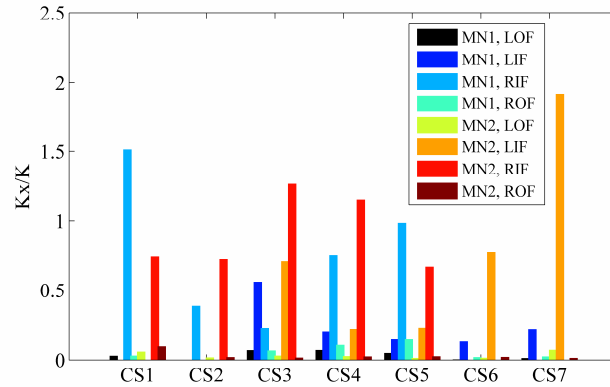
Fig.18 Streamwise variation of K_x / K at centerlines of the inside floodplain and the outside floodplain ("LOF", "LIF", "RIF" and "ROF" indicates "Left Outside Floodplain", "Left Inside Floodplain", "Right Inside Floodplain" and "Right Outside Floodplain")

8.2 Sensitivity analysis of panel number

The panel divided theory (shown in Section 3) is important to the prediction of depth-averaged velocity. In order to explore the sensitivity of the proposed model to the number of divided panels, the recommended panels, (i.e., the outside floodplain, the inside floodplain, the mixing region next to the inner and outer side walls), are all ignored and only three panels (the left floodplain, the main channel and the right floodplain) are used herein. Three typical cross-sections are selected which are the middle section of a meander bend (CS1), the exit of a meander bend (CS3) and the entrance of a meander bend (CS5). In the three sections, the velocity parameter on the floodplain is set as 0.7 on both left and right floodplains while in the main channel K is selected as 1.6, 1.7

and 1.8 in CS1, CS3 and CS5, respectively. The predictions with 3 panels and 7 or 9 panels are

shown in Fig.19. From the figure, with only three panels, the prediction on the floodplain is nearly

a constant which cannot reflect the increased U_d on the outside floodplains. Besides, in the main

channel, poor predictions are obtained by ignoring mixing regions, particularly in CS3 and CS5.

Therefore, the region divided number affects the accuracy of this model. Use of fewer panels may

provide convenience for calculation, but leads to poor prediction because in this case some typical

flow characteristics are almost ignored.

(a)CS1

(b)CS3

(c)CS5
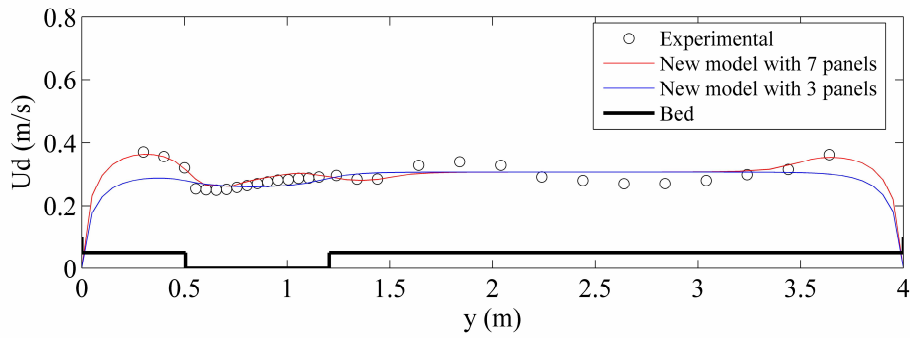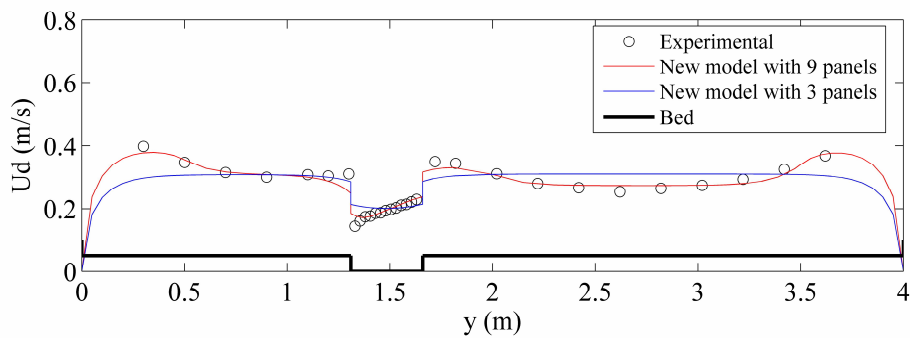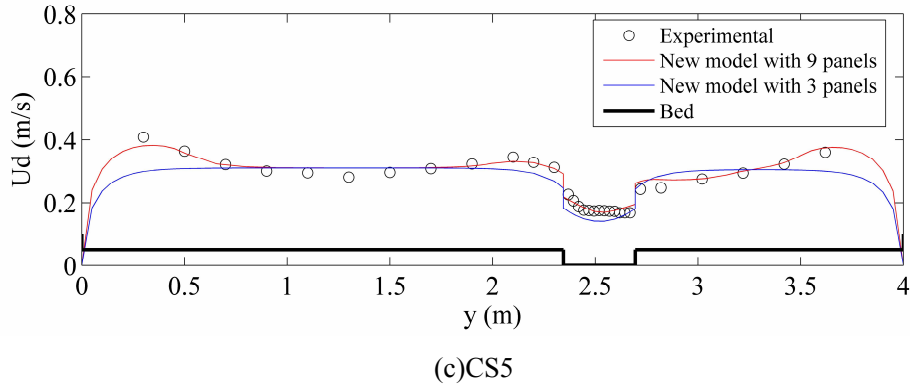
Fig.19 Effect of panel divided number on lateral depth-averaged velocity distribution at three

typical cross-sections, based on experimental data of case MN1, H=0.255m, Q=0.189 m³/s

8.3 Limitation of the proposed model

It is worth noting the limitations of the proposed model. All equations were derived and two group

experiments were done under the hypothesis of quasi-uniform flow. For the other flow conditions,

the feasibility of governing equation (Eq.(5)) and secondary flow equations (Eqs.(7)-(9)) along a

meander warrant further study. In the meandering compound channel, the growth and decay of

secondary flow in the main channel are clarified in Figs.7-8. From the analysis and discussion of

the components in velocity term, the velocity parameter has been demonstrated as a lateral and

longitudinal variable. Setting the velocity parameter in the real ranges calculated by experimental

data, the good predictions of depth-averaged velocity are obtained along half a meander,

particularly in cross-over sections, which indicates the proposed model is reasonable. However, in

the channels with mobile bed and flood plain vegetation, the generation mechanism and

distribution of secondary flow are quite different which lead to significant variations of the bed

form. Further, the bed morphology considerably affects the longitudinal distribution of

depth-averaged velocity. These changes of bed roughness cause that the velocity parameter (K) is

much harder to determine and the calibration may be a method to obtain its value. In addition, the additional resistances of mobile bed and flood plain vegetation also deflect the flow direction, hence, the boundary conditions and the angles have to be reconsidered.

9. Conclusions

This paper presents an analytical model under quasi-uniform flow to model the lateral distributions of depth-averaged velocity for half a meander in the curved compound channel. This model defines the velocity term in the governing equation, which includes both the streamwise velocity variation and the lateral secondary flow variation. In the meandering main channel, the generation mechanism of secondary flows is analyzed, finding that the effect of centrifugal force and floodplain flow must be considered, especially at the cross-over sections. New expressions for velocity variation parameters are proposed in the main channel and on the floodplain. Whilst using the method on each test case requires initial calibration, once this is done, the method is very useful in identifying key processes and demonstrating their importance and it can predict results at other depths for that same geometry.

Two experiments (MN1 and MN2) were conducted in a large scale meandering compound channel. The three dimensional velocity components, the Reynolds shear stress and the stage-discharge were measured at seven designed test sections along half a meander (CS1 to CS7 shown in Fig.2). The experimental data of transverse velocity along half a meander demonstrate that the analysis of the secondary flow's generation mechanism in the meandering main channel is accurate and reasonable.

The main channel considered here is rectangular, leading to a discontinuity of flow depth at the interfaces of the main channel and its corresponding floodplains. Further, the effect of the meandering main channel flow to the inside floodplain flow must be considered while it may be ignored to the outside floodplain flow. Hence, the divided region method for each test section was proposed here.

The parameters corresponding to the effects of lateral momentum transfer, bed friction and secondary flow are introduced. Based on the experimental data, some new findings about the dimensionless eddy viscosity (λ_{mc}) in the main channel are obtained, showing that its value at the apex section is still equal 0.07, but λ_{mc} value ranges from 0.033 to 0.05 at the cross-over sections. On the floodplain, back calculated values (0.132 and 0.121) are used for both cases MN1 and MN2, respectively.

The new boundary condition, considering the relation of velocities in the main channel and on the floodplain, was proposed based on the angles (shown in Fig.10). At the cross-over sections (CS2-CS6), the angle (θ) between the meandering main channel and the floodplain was divided into two angles which are related to the velocity continuity and the velocity gradient continuity. From the modeled work, poor results are obtained at the cross-over sections, when neglecting the influence of angles ($\theta_1 = \theta_2 = 0°$) in Eq.(17) demonstrating the importance of the inclusion of these angles proposed in this paper.

Finally, the modeling depth-averaged velocity distributions along half a meander were compared with the experimental data. The modeling capability of the proposed model in both cases (MN1 and MN2) is excellent, whether at the apex sections (CS1 and CS7) or the cross-over ones (CS2 to CS6), by adopting the new boundary conditions and considering both the streamwise velocity variation and lateral secondary flow variation. If more experimental data and field data, including flow depths, bed slopes, meander belt widths, channel bed conditions and sinuosity can be obtained; further verification of this model may be made.

Notation

The following symbols are used in this paper:

A_1, A_2, = integration constants in Eq.(15);

B = total width;

b = main channel width;

Dr $=$ relative depth, $(H\text{-}h)/H$;

F_c $=$ centrifugal force;

f $=$ Darcy-Weisbach friction factor;

g $=$ local gravitational acceleration;

H $=$ flow depth;

h $=$ bankfull level;

K $=$ velocity variation parameter, defined by Eqs.(7)-(9);

K_x $=$ streamwise variation coefficient;

K_{y1}, K_{y2} $=$ secondary flow coefficients;

n $=$ Manning's coefficient;

R $=$ hydraulic radius;

S $=$ valley slope;

U,V,W $=$ velocity components corresponding to the x,y,z directions;

U_d $=$ depth-averaged streamwise velocity, defined by Eq.(2);

$U_{d(1)}$ $=$ depth-averaged velocity on the floodplain, shown in Fig.10;

$U_{d(2)}$ $=$ projection of $U_{d(3)}$ in the streamwise direction on the floodplain, shown in Fig.10;

$U_{d(3)}$ $=$ depth-averaged velocity in the main channel with the true flow direction, shown in Fig.10;

$U_{d(4)}$ $=$ measured experimental depth-averaged velocity following the valley direction in the main channel, shown in Fig.10;

U_* $=$ shear velocity, defined by Eq.(6);

V_1 $=$ transverse velocity without effect of centrifugal force;

V_2 = component of floodplain flow;

x,y,z = streamwise, lateral and vertical coordinates, respectively;

λ = dimensionless eddy viscosity;

ω = Coefficients in Eq.(15);

$\bar{\varepsilon}_{yx}$ = depth-averaged eddy viscosity, defined by Eq.(6);

θ = angle at the cross-over section ($=\theta_1 + \theta_2$), shown in Fig.10;

θ_1 = Angle between $U_{d(3)}$ and $U_{d(4)}$, shown in Fig.10;

θ_2 = angle between $U_{d(2)}$ and $U_{d(3)}$, shown in Fig.10;

τ_b = bed shear stress;

$\bar{\tau}_{yx}$ = depth-averaged Reynolds shear stress;

τ_{yx}, τ_{zx} = Reynolds shear stresses on the planes perpendicular to y and z, respectively; and

ρ = flow density.

Subscripts

H = flow height;

h = bankfull height;

H-h = floodplain;

mc = main channel; and

fp = floodplain.

References

[1] Abril JB, Knight DW. Stage discharge prediction for rivers in flood applying a depth

averaged model. Journal of Hydraulic Research 2004; 42(6): 616-629. http://dx.doi.org/10.1080/00221686.2004.9628315

[2] Cao Z, Meng J, Penderand G., Wallis S. Flow resistance and momentum flux in compound open channels, Journal of Hydraulic Engineering 2006; 132(12): 1272-1282. http://dx.doi.org/10.1061/(ASCE)0733-9429(2006)132:12(1272)

[3] Carling PA., Cao Z, Holland MJ, Ervine DA, Babaeyan-Koopaei K. Turbulent flow across a natural compound channel, Water Resources Research 2002; 38(12): Article Number 1270. http://dx.doi.org/10.1029/2001WR000902

[4] Castanedo S, Medina M, Mendez FJ. Models for the turbulent diffusion terms of shallow water equations, Journal of Hydraulic Engineering 2005; 131(3): 217-223. http://dx.doi.org/10.1061/(ASCE)0733-9429(2005)131:3(217)

[5] Ervine DA, Willetts BB, Sellin RHJ, Lorena M. Factors affecting conveyance in meandering compound flows, Journal of Hydraulic Engineering 1993; 119(12): 1383-1399. http://dx.doi.org/10.1061/(ASCE)0733-9429(1993)119:12(1383)

[6] Ervine DA, Babaeyan-koopaei K, Sellin RHJ. Two-dimensional solution for straight and meandering overbank flows, Journal of Hydraulic Engineering 2000; 126(9): 653-669. http://dx.doi.org/10.1061/(ASCE)0733-9429(2000)126:9(653)

[7] Greenhill RK, Sellin RHJ. Development of a simple method to predict discharges in compound meandering channels, Proceedings of the Institution of Civil Engineers Water, Maritime & Energy 1993; 101: 37-44. http://dx.doi.org/10.1680/iwtme.1993.22986

[8] Hu CH, Ji ZW, Guo QC. Flow movement and sediment transport in compound channels, Journal of Hydraulic Research 2010; 48(1): 23-32.

http://dx.doi.org/10.1080/00221680903568600

[9] Huai WX, Xu ZG, Yang ZH, Zeng YH. Two dimensional analytical solution for a partially vegetated compound channel flow, Applied Mathematics and Mechanics 2008; 29(8): 1077-1084. http://dx.doi.org/10.1007/s10483-008-0811-y

[10] Huai WX, Gao M, Zeng YH, Li D. Two-dimensional analytical solution for compound channel flows with vegetated floodplain, Applied Mathematics and Mechanics 2009; 30(9): 1049-1056. http://dx.doi.org/10.1007/s10483-009-0906-z

[11] Ishigaki T, Shiono K, Rameshwaran P, Scott CF, Muto Y. Impact of secondary flow on bed form and sediment transport in a meandering channel for overbank flow, Annual Journal of Hydraulic Engineering, JSCE, 2000; 44: 849-854. http://dx.doi.org/10.2208/prohe.44.849

[12] Jing H, Guo Y, Li C, Zhang J. Three-dimensional numerical simulation of compound meandering open channel flow by the Reynolds stress model, International Journal for Numerical Methods in Fluids, 2009; 59: 927-943. http://dx.doi.org/10.1002/fld.1855

[13] Keevil GM., Peakall J, Best JL, Amos KJ. Flow structure in sinuous submarine channels: Velocity and turbulence structure of an experimental submarine channel, Marine Geology 2006; 229: 241-257. http://dx.doi.org/10.1016/j.margeo.2006.03.010

[14] Knight DW, Demetriou JD. Flood plain and main channel flow interaction, Journal of Hydraulic Engineering 1983; 109(8): 1073-1092. http://dx.doi.org/10.1061/(ASCE)0733-9429(1983)109:8(1073)

[15] Knight DW, Sellin RHJ. The SERC flood channel facility. Journal of the Institution of Water and Environmental Management 1987; 41(4): 198-204. http://dx.doi.org/10.1111/j.1747-6593.1987.tb01212.x

[16] Knight DW, Omran M, Abril JB. Boundary conditions between panels in depth-averaged flow models revisited. River Flow, Proceedings of 2nd International Conference on Fluvial Hydraulics, 2004; 23–25 June, Napoli, Italy, Vol. 1, 371-380.

[17] Knight DW, Omran M, Tang X. Modeling Depth-Averaged Velocity and Boundary Shear in Trapezoidal Channels with Secondary Flows, Journal of Hydraulic Engineering 2007; 133(1): 39-47. http://dx.doi.org/10.1061/(ASCE)0733-9429(2007)133:1(39)

[18] Knight DW, Tang X, Sterling M, Shiono K, Mc Gahey C. Solving open channel flow problems with a simple lateral distribution model, In Riverflow 2010, Proceedings of the International Conference on Fluvial Hydraulics, Braunschweig, Germany (pp. 41-48).

[19] Lambert MF, Sellin RHJ. Velocity Distribution in a Large-Scale Model of a Doubly Meandering Compound River Channel. Proceedings of the Institution of Civil Engineers Water, Maritime and Energy, 1996; 118(1): 10-20. http://dx.doi.org/10.1680/iwtme.1996.28161

[20] Liu C, Luo X, Liu XN, Yang KJ. Modeling depth-averaged velocity and bed shear stress in compound channels with emergent and submerged vegetation. Advances in Water Resources, 2013; 60: 148-159. http://dx.doi.org/10.1016/j.advwatres.2013.08.002

[21] Lyness JF, Myers WRC, Cassells JBC, O'sullivan JJ. The influence of planform on flow resistance in mobile bed compound channels, Proceedings of the Institution of Civil Engineers Water and Maritime Engineering 2001; 148: 5-14. http://dx.doi.org/10.1680/wame.2001.148.1.5

[22] Martin-Vine JP, Moreta PJM, Lopez-Querol S. Improved 1-D modeling in compound meandering channels with vegetated floodplains, Journal of Hydraulic Research 2008; 46(2):

265-276. http://dx.doi.org/10.1080/00221686.2008.9521860

[23] McGahey C, Samuels PG. Methodology for conveyance estimation in two-stage straight, skewed and meandering channels, Proceedings of the XXX Congress of the International Association for Hydraulic Research, 2003; Vol. C1: 33-40, Thessaloniki, Greece.

[24] Morvan H, Pender G, Wright NG, Ervine DA. Three-dimensional hydrodynamics of meandering compound channels, Journal of Hydraulic Engineering 2002; 128(7): 674-682. http://dx.doi.org/10.1061/(ASCE)0733-9429(2002)128:7(674)

[25] Pasche E, Rouve GM. Overbank flow with vegetatively roughened flood plains, Journal of Hydraulic Engineering 1985; 111(9): 1262-1278. http://dx.doi.org/10.1061/(ASCE)0733-9429(1985)111:9(1262)

[26] Patra KC, Kar SK. Flow interaction of meandering river with floodplains, Journal of Hydraulic Engineering 2000; 126(8): 593-604. http://dx.doi.org/10.1061/(ASCE)0733-9429(2000)126:8(593)

[27] Patra KC, Kar SK, Amartya KB. Flow and velocity distribution in meandering compound channels, Journal of Hydraulic Engineering 2004; 130(5): 398-411. http://dx.doi.org/10.1061/(ASCE)0733-9429(2004)130:5(398)

[28] Rameshwaran P, Spooner J, Shiono K, Chandler JH. Flow Mechanisms in two-stage meandering channel with mobile bed, Process 28th Congress of IAHR, 1999; Vol. 256: 259-266, Graz, Austria.

[29] Rameshwaran P, Shiono K. Quasi two-dimensional model for straight overbank flows through emergent vegetation on floodplains, Journal of Hydraulic Research 2007; 45(3): 302-315. http://dx.doi.org/10.1080/00221686.2007.9521765

[30] Shao X, Wang H, Chen Z. Numerical modeling of turbulent flow in curved channels of compound cross-section, Advances in Water Resources 2003; 26: 525-539. http://dx.doi.org/10.1016/S0309-1708(03)00008-3

[31] Shiono K, Knight DW. Turbulent open channel flows with variable depth across the channel, Journal of Fluid Mechanics 1991; 222: 617-646. http://dx.doi.org/10.1017/S0022112091001246

[32] Shiono K, Muto Y. Complex flow mechanisms in compound meandering channel for overbank flow, Journal of Fluid Mechanics 1998; 376: 221-261. http://dx.doi.org/10.1017/S0022112098002869

[33] Shiono K, Muto Y, Knight DW, Hyde AFL. Energy losses due to secondary flow and turbulence in meandering channel for overbank flows, Journal of Hydraulic Research 1999; 37(5): 641-664. http://dx.doi.org/10.1080/00221689909498521

[34] Shiono K, Al-Romaih JS, Knight DW. Stage-discharge assessment in compound meandering channels, Journal of Hydraulic Engineering 1999; 125(1): 66-77. http://dx.doi.org/10.1061/(ASCE)0733-9429(1999)125:1(66)

[35] Shiono K, Spooner J, Chan TL, Rameshwaran P, Chandler JH. Flow characteristics in meandering channels with non-mobile and mobile beds for overbank flows, Journal of Hydraulic Research 2008; 46(1): 113-132. http://dx.doi.org/10.1080/00221686.2008.9521848

[36] Shiono K, Chan TL, Spooner J, Rameshwaran P, Chandler JH. The effect of floodplain roughness on flow structures, bedforms and sediment transport rates in meandering channels with overbank flows: Part I, Journal of Hydraulic Research 2009; 47(1): 5-19. http://dx.doi.org/10.3826/jhr.2009.2944-I

[37] Shiono K, Chan TL, Spooner J, Rameshwaran P, Chandler JH. The effect of floodplain roughness on flow structures, bedforms and sediment transport rates in meandering channels with overbank flows: Part II, Journal of Hydraulic Research 2009; 47(1): 20-28. http://dx.doi.org/10.3826/jhr.2009.2944-II

[38] Spooner J. Flow structures in a compound meandering channel with flat and natural bedforms, 2001; Ph.D. thesis, Loughborough University, U.K.

[39] Tang X, Knight DW. A general model of lateral depth-averaged velocity distributions for open channel flows, Advances in Water Resources 2008; 31: 846-857. http://dx.doi.org/10.1016/j.advwatres.2008.02.002

[40] Tang X, Knight DW. Analytical models for velocity distributions in open channel flows, Journal of Hydraulic Research 2009; 47(4): 418-428. http://dx.doi.org/10.1080/00221686.2009.9522017

[41] Tominaga A, Nezu I, Ezaki K, Nakagawa H. Three-dimensional turbulent structure in straight open channel flows, Journal of Hydraulic Research 1989; 27(1): 149-173. http://dx.doi.org/10.1080/00221688909499249

[42] Wormlemeaton PR, Sellin RHJ, Bryant T, Loveless JH, Hey RD, Catmur SE. Flow structure in a two-stage channel with a mobile bed, Journal of Hydraulic Research 2004; 42(2): 145-162. http://dx.doi.org/10.1080/00221686.2004.9728378

[43] Yang KJ, Cao SY, Knight DW. Flow patterns in compound channels with vegetated floodplains, Journal of Hydraulic Engineering 2007; 133(2): 148-159. http://dx.doi.org/10.1061/(ASCE)0733-9429(2007)133:2(148)

[44] Yang KJ, Nie RH, Liu XN, Cao SY. Modeling depth-averaged velocity and boundary shear

stress in rectangular compound channels with secondary flows, Journal of Hydraulic Engineering 2013; 139(1): 76-83. http://dx.doi.org/10.1061/(ASCE)HY.1943-7900.0000638

[45] Yuen KWH. A study of boundary shear stress, flow resistance and momentum transfer in open channels with simple and compound trapezoidal cross sections, 1989; Ph.D. thesis, University of Birmingham, U.K.

[46] Zarrati AR, Tamai N, Jin YC. Mathematical modeling of meandering channels with a generalized depth averaged model, Journal of Hydraulic Engineering 2005; 131(6): 467-475. http://dx.doi.org/10.1061/(ASCE)0733-9429(2005)131:6(467)